Glucocorticoid-driven mitochondrial damage stimulates Tau pathology

Fang Du,[1,†] Qing Yu,[1,†] Russell H. Swerdlow[2] and Clarissa L. Waites[1,3]

[†]**These authors contributed equally to this work.**

Abstract

Prolonged exposure to glucocorticoids, the main stress hormones, damages the brain and is a risk factor for depression and Alzheimer's disease. Two major drivers of glucocorticoid-related neurotoxicity are mitochondrial dysfunction and Tau pathology; however, the molecular/cellular mechanisms precipitating these events, and their causal relationship, remain unclear.

Using cultured murine hippocampal neurons and 4-5-month-old mice treated with the synthetic glucocorticoid dexamethasone, we investigate the mechanisms underlying glucocorticoid-induced mitochondrial damage and Tau pathology.

We find that glucocorticoids stimulate opening of the mitochondrial permeability transition pore via transcriptional upregulation of its activating component, Cyclophilin D. Inhibition of Cyclophilin D is protective against glucocorticoid-induced mitochondrial damage as well as Tau phosphorylation and oligomerization in cultured neurons. We further identify the mitochondrially-targeted compound mito-apocynin as an inhibitor of glucocorticoid-induced permeability transition pore opening, and show that this compound protects against mitochondrial dysfunction, Tau pathology, synaptic loss, and behavioral deficits induced by glucocorticoids *in vivo*. Finally, we demonstrate that mito-apocynin and the glucocorticoid receptor antagonist mifepristone rescue Tau pathology in cytoplasmic hybrid cells, an *ex vivo* Alzheimer's disease model wherein endogenous mitochondria are replaced with mitochondria from Alzheimer's subjects.

These findings show that mitochondrial permeability transition pore opening is a precipitating factor in glucocorticoid-induced mitochondrial dysfunction, and that this event stimulates Tau pathogenesis. Our data also link glucocorticoids to mitochondrial dysfunction and Tau pathology in the context of Alzheimer's disease, and suggest that mitochondria are promising therapeutic

targets for mitigating stress- and Tau-related brain damage.

Author affiliations:

1 Department of Pathology and Cell Biology, Taub Institute for Research on Alzheimer's Disease and Aging Brain, Columbia University Irving Medical Center, New York, NY 10032, USA

2 University of Kansas Alzheimer's Disease Center, University of Kansas School of Medicine, Landon Center on Aging, Kansas City, KS, 66103, USA

3 Department of Neuroscience, Columbia University, New York, NY, 10032, USA

Correspondence to: Clarissa Waites, PhD

650 W. 168th St., Black Building 1210B, New York, NY 10032, USA

E-mail: cw2622@cumc.columbia.edu

Running Title: Glucocorticoids, mitochondria, and Tau pathology

Keywords: glucocorticoids; stress; mitochondria; tau; mPTP; cyclophilin D

Abbreviations: CDK5 = Cyclin-dependent kinase 5; CORT = corticosterone; CsA = Cyclosporin A; CypD = Cyclophilin D; Dex = Dexamethasone; EPM = Elevated plus maze; ERK1/2 = Extracellular signal-regulated kinases; FST = Forced swimming test; GC = Glucocorticoids; GR = Glucocorticoid receptor; GREs = Glucocorticoid response elements; GSK3 = Glycogen synthase kinase 3; mAPO = Mito-apocynin; MIF = Mifepristone; mPTP = Mitochondrial permeability transition pore; mROS = Mitochondrial reactive oxygen species; NADPH = Nicotinamide adenine dinucleotide phosphate; PFC = prefrontal cortex

Introduction

The release of glucocorticoids (GCs) in response to acute stress triggers the fight-or-flight response, which mobilizes the body's resources to escape from danger and is essential for survival. However, GC release in response to chronic stress has profoundly detrimental effects on mammalian physiology and brain health in particular. Pathophysiological levels of GCs cause atrophy of the hippocampus and prefrontal cortex, with accompanying deficits in learning, memory, and mood regulation,[1,2] and are a risk factor for depression and Alzheimer's disease.[3-6] It was recently shown that stress/GC-related brain atrophy and behavioral deficits are mediated by the microtubule-associated protein Tau, as Tau knockout mice do not develop these stress/GC-induced phenotypes.[7,8] Importantly, the intraneuronal accumulation and aggregation of Tau is a shared pathogenic mechanism between stress-induced brain pathology and neurological diseases including Alzheimer's, progressive supranuclear palsy, Pick disease, chronic traumatic encephalopathy, and epilepsy.[9-11] Although Tau aggregates are a hallmark of these disorders, it is increasingly recognized that Tau toxicity is primarily mediated by oligomers, composed of Tau species formed early in the aggregation process.[9,12,13]

The cellular mechanisms by which stress/GCs induce Tau oligomerization remain poorly understood. Hyperphosphorylation of Tau is one driver of its oligomerization, and GCs are known to activate major Tau kinases, including GSK3, CDK5, and ERK1/2.[14-17] In addition, Tau proteolysis generates C-terminally truncated species of Tau that potentiate its oligomerization,[9] and chronic stress enhances caspase 3-mediated truncation of Tau at its C-terminus.[18] Moreover, GCs promote Tau accumulation through their inhibition of major cellular degradative pathways (autophagy and the endolysosomal pathway) and dysregulation of molecular chaperones Hsp70 and Hsp90.[18-20] However, it is unclear which if any of these events are the main drivers of GC-induced Tau oligomerization.

Once formed, Tau oligomers interfere with multiple aspects of neuronal function, including synaptic transmission, genome stability, protein clearance, and axonal transport.[9,12] Notably, pathogenic Tau also inhibits neuronal energy production by altering mitochondrial transport, fission/fusion, respiratory activity, and membrane potential.[21-26] In addition, oligomeric Tau may promote opening of the mitochondrial permeability transition pore (mPTP),[27,28] a channel on the inner mitochondrial membrane whose sustained opening causes mitochondrial dysfunction and

can trigger apoptosis.[29] Although Tau oligomers clearly impede mitochondrial function, there is also evidence that mitochondrial dysfunction promotes Tau oligomerization and drives Tau pathology in Alzheimer's disease,[30-32] showing that these processes are tightly intertwined, although their mechanistic relationship is uncertain.

Mitochondria are major targets of GC regulation, and have their own glucocorticoid receptors (GRs) that modulate mitochondrial DNA transcription in response to GC binding.[33] As the organelles responsible for energy production to sustain the stress response, as well as the production and metabolism of GCs and other steroid hormones, mitochondria are highly sensitive to GC levels.[34] GCs have a biphasic effect on neuronal mitochondria, enhancing Ca^{2+} buffering and maintaining mitochondrial membrane potential at physiological levels, but impairing these functions under sustained pathophysiological levels.[35] In addition, high GC levels have detrimental effects on mitochondrial quality control, altering mitochondrial fission/fusion, suppressing genes involved in mitophagy and mitochondrial biogenesis, and promoting the accumulation of damaged mitochondria.[33] While GCs impact multiple aspects of mitochondrial health and function as well as Tau accumulation and oligomerization, the mechanistic relationship between stress/GCs, mitochondrial damage, and Tau pathology remains unclear.

In the current study, we examine this relationship using cultured hippocampal neurons, murine hippocampus, and cytoplasmic hybrid (cybrid) cells containing mitochondria from Alzheimer's subjects and age-matched controls.[30] We find that GCs induce mPTP opening via upregulation of cyclophilin D (CypD), an activating component of the mPTP.[29] Inhibiting CypD activity or expression in cultured neurons prevents Tau phosphorylation and oligomerization, indicating that mPTP opening drives Tau pathology. Moreover, inhibiting mPTP opening and mitochondrial damage *in vivo* with the mitochondrially-targeted compound mito-apocynin ameliorates GC-driven behavioral impairment, synapse loss, and Tau pathology in the hippocampus. Mito-apocynin and the GR antagonist mifepristone similarly rescue Tau pathology in Alzheimer's cybrid cells, further supporting the concept that GC-related mitochondrial dysfunction drives Tau pathogenesis in the context of chronic stress and Alzheimer's disease. These findings shed light on the mechanism of stress/GC-induced Tau oligomerization and the critical role of mitochondria in this process.

Materials and methods

Animals

4-5-month-old wild-type C57 mice of both sexes (obtained from National Institute of Aging) were maintained under standard laboratory conditions with ad libitum access to food and water. All animal studies were carried out with the approval of the Columbia Institutional Animal Care and Use Committee (IACUC) in accordance with the National Institutes of Health guidelines for animal care. Mice were randomly divided into 4 groups (control, dexamethasone, dexamethasone + mifepristone, dexamethasone + mito-apocynin) of 9-10 animals per group. Animal numbers (n) for experiments were obtained based on the estimated effect sizes calculated in our previous study and those published by other research groups.[7,20,36] This estimation uses a significance level of 0.05, mean group difference of 25-35%, and SD values within the 30-40% range from the known mean of the population, and a power test of 0.80. While this analysis yields a group size of 4-6 for single-sex experiments (as used for behavioral testing), we used additional animals to account for the intrinsic inter-animal variability typically observed in mice and to ensure that statistically valid behavioral results were obtained. Animals were administered the following drugs: dexamethasone (D2915, Sigma; 5mg/kg per day, dissolved in PBS, by intraperitoneal/i.p. injection), mito-apocynin (HY-135869, MedChemExpress; 3mg/kg per day, dissolved in 15% polyethylene glycol/PEG400 with PBS, by oral gavage) and mifepristone/RU486 (S2606, Selleckchem; 10mg/kg per day, dissolved in 50% PEG400 in PBS, by i.p.). Control animals received daily i.p. injections of 50% PEG400 in PBS (dex/mifepristone vehicle) and oral gavage of 15% PEG400 with PBS (mito-apocynin vehicle). All treatments were administered for 15 consecutive days, typically between 10-10:30am (during the animals' light phase). During the behavioral testing period (3 days), drugs were administered at ~5pm after testing had concluded.

Behavioral Testing

Male mice were subject to behavioral testing in the following order: EPM, Y-maze, FST. Each test was carried out on a single day between 9am and 4pm. For each test, animals were randomly divided into two groups (each balanced for all 4 treatment conditions), with half tested in the morning and half in the afternoon. Animals from the different treatment conditions were alternated

for each behavioral trial.

Elevated plus maze (EPM). The apparatus used for the EPM test consists of two open arms (30 cm × 5 cm) across from each other and perpendicular to two closed arms (30 cm × 5 cm) with a center platform (5 cm × 5 cm)[37]. The entire apparatus is 50 cm above the floor. Experimental mice were acclimated to the behavior room (illumination 30 lux) for 30 min prior to testing. Each mouse was placed in the center platform facing an open arm to start the trial, and was allowed to explore the maze for 5 min. The apparatus was cleaned with 70% ethanol between animals. Photobeams embedded at arm entrances registered movements, which were automatically scored by MED-PC V Software (Med Associates).

Y-maze spontaneous alternation. The Y-maze consists of three identical arms at 120°C angles from one other. Each mouse was placed in the center of the maze and allowed to explore freely for 8 min. The apparatus was cleaned with 70% ethanol between animals. Trials were videotaped and analyzed by Ethovision XT software, with the total number of arm entries, as well as the sequence of entries, calculated to obtain the percentage of alternations (defined as entries into a different arm than the one previously explored).[38]

Forced swimming test (FST). Mice were individually placed in a transparent cylindrical glass container (50 cm height, 20 cm diameter) filled with 40 cm water at 27°C ± 2°C. Experimental mice were acclimated to the behavior room (illumination 30 lux) for 30 min prior to testing. Each mouse was gently placed into the water for 6 min, then removed from the cylinder and dried immediately. The test period was divided into pretest (first 2 min) and test (last 4 min). Between trials, the cylinder was emptied, rinsed, and refilled with fresh water. Test trials were videotaped and analyzed by Ethovision XT software, with "immobility duration" defined as the portion of the test period spent floating with the absence of any movement except for that necessary to keep the animal's nose above water.[39]

Evaluation of serum corticosterone (CORT) levels

Blood samples were collected between 2-3pm following decapitation, 4 hours after the final administration of Dex/vehicle on day 15. Endogenous CORT serum levels were measured using the Corticosterone Parameter Assay (ELISA) kit (R&D Systems, KGE009). The wavelength for

measurement was 450 nm and the correction wavelength was 570 nm.

Hippocampal neuronal culture

Hippocampal neurons from postnatal day 1 male and female mice were prepared as previously described,[40] and maintained in Neurobasal medium supplemented with B27, 600 μM L-glutamine, and penicillin–streptomycin (all from ThermoFisher/Life Technologies). At 11 days *in vitro* (DIV), neurons were transfected with siRNAs against CypD/*Ppif* (ThermoFisher, s98515) or control siRNAs (sc-37007, Santa Cruz) for 72 hours prior to experiments. At 11 or 12 DIV, neurons were treated with the following drugs for 48 hours prior to experiments: dexamethasone (D2915, Sigma; 1μM), mifepristone/RU486 (S2606, Selleckchem; 5μM), mito-apocynin (HY-135869, MedChemExpress, 1μM), cyclosporin A (C1832, Sigma, 1 mM). Primary neuronal cultures were collected for immunoblotting or immunostaining at 14 DIV.

Cybrid cell creation and differentiation

Alzheimer's disease and non-Alzheimer's cybrid cells were generated by and provided through the University of Kansas Alzheimer's Disease Center (KUADC) Mitochondrial Genomics and Metabolism Core. Cybrid cell lines were created in human neuroblastoma cells (SH-SY5Y) depleted of endogenous mtDNA (Rho^0 cells), which were then fused with platelet cytoplasm from human donors, and repopulated with mitochondria containing mtDNA from Alzheimer's subjects or age-matched controls as previously described.[41,42] Subjects and controls were recruited through the KUADC. Subjects met the National Institute of Neurological and Communicative Disorders and Stroke and the Alzheimer's Disease and Related Disorders Association criteria.[43] Controls were cognitively normal and age-matched to subjects. All subjects and controls provided written informed consent to participate in the study. We used 4 cell lines per group in this study and the ages of subject and control platelet donors were 75.5 ± 6.50 and 78.5 ± 3.77 years, respectively. Detailed information about gender, age, and disease status of donors is included in **Supplementary Table 1** and in previous studies.[44-46] Alzheimer's and control cybrid cells were grown in DMEM supplemented with 10% fetal bovine serum (FBS; Gibco BRL, Logan, Utah), 100 μg/ml pyruvate,

50 µg/ml uridine, and antibiotic-antimycotic as previously described.[32,45,47] Staurosporine (ab120056, Abcam) was used to differentiate SH-SY5Y cybrid cells into a neuronal phenotype with the appearance of neurite-like processes.[48] Culture medium was replaced with differentiation media (Neurobasal media supplemented with B27, 0.5 mM glutamine, antibiotic-antimycotic, and 10 nM staurosporine) for 14 days, with half of the differentiation media replaced every day as previously described.[32,44,45,47]

DNA and lentivirus production

Full-length human cyclophilin D (gene name *PPIF;* NCBI accession #NM_005729.4) was synthesized at Genewiz/Azenta and subcloned into pEGFP-C2 vector (Clontech) at the EcoRI site. EGFP-CypD was then subcloned into pFUGWm lentiviral vector using compatible ends digests Mfe1/Nhe1 (pEGFP-C2) and EcoRI/Xba1 (pFUGWm) to create pFUGCypDW. Lentivirus was produced in HEK293T cells from pFUGWm (for GFP control) or pFUGCypDW plasmids as previously described.[49,50] Neurons were transduced with 50-150 ml of lentiviral supernatant per well (12-well plates) or 10-40 ml per coverslip (24-well plates) at 10 DIV for overexpression experiments.

Immunoblotting

Protein extracts were separated by SDS/PAGE (10% Tris-Glycine gel; XP00105BOX, Invitrogen), and then transferred to a nitrocellulose membrane (10600001, Amersham). After blocking in TBST buffer (20 mM Tris-HCl, 150 mM sodium chloride, 0.1% Tween-20) containing 5% (wt/vol) nonfat dry milk for 1 h at room temperature, the membrane was incubated with primary antibodies overnight at 4°C, then with secondary antibodies for 1 h at room temperature. The following antibodies were used: Tau5 (ab80579, Abcam), AT8: anti-phospho-Tau pSer202/Thr205 (MN1020, Thermo Fisher Scientifc), PHF-1: anti-phospho-Tau pSer396/Ser404 Tau (from Dr. Peter Davies), anti-CypD (ab110324, Abcam), anti-Tubulin (ab4074, Abcam), anti-Tom20 (F-10; sc-17764, Santa Cruz), anti-OSCP (A-8; sc-365162, Santa Cruz), IRDye 800CW goat anti-mouse IgG secondary antibody (P/N: 926-32210, LI-COR), IRDye 680CW goat anti-

rabbit IgG secondary antibody (P/N: 926-68071, LI-COR). Membranes were visualized by Odyssey Infrared Imager (model 9120, LI-COR Biosciences), and relative optical densities of bands determined by Fiji/ImageJ software and normalized to Tubulin.

Mitochondria functional assays

Complex I activity and ATP production were measured from 14 DIV hippocampal neurons or hippocampal tissue with Complex I Enzyme Activity Microplate Assay Kit (ab109721, Abcam) and ATP Assay Kit (Colorimetric/Fluorometric, ab83355, Abcam), respectively, according to manufacturer's instruction. To estimate production of reactive oxygen species (ROS), brain sections from mouse hippocampal tissue or primary neurons were plated onto Lab-Tek 4-well chamber slides (177437, Lab-Tek) and exposed to 1 µM MitoSOX Red (M36008, ThermoFisher), a fluorochrome specific for anion superoxide produced in the inner mitochondrial compartment, at 37°C for 30 minutes. For visualization of mitochondria, cells were co-stained with MitoTracker Green FM (100 nM, 9074, Cell signaling) at 37°C for 30 minutes before fixation as described.[51] To visualize the colocalization between MitoSOX and oligomeric Tau, hippocampal slices, cultured neurons and cybrids were incubated with MitoSOX, then fixed and immunostained with anti-oligomeric Tau antibody TOMA-1 (for hippocampal slices and cultured neurons, details described in Immunofluorescence staining) or anti-oligomeric Tau antibody T22 (for cybrid cells, details described in Immunofluorescence staining). To assess mitochondrial membrane potential, brain sections or neurons plated onto Lab-Tek chamber slides were stained with tetramethylrhodamine methyl ester (TMRM, 100 nM, ab275547, Abcam) at 37°C for 30 minutes. Images were acquired at 37°C with a 40X oil-immersion objective (Neofluar, NA 1.3) on an epifluorescence microscope (Axio Observer Z1, Zeiss) with Colibri LED light source, EMCCD camera (Hamamatsu) and Zen 2012 (blue edition) software. Quantification of staining intensity and the percentage of area occupied by Mitosox was measured and quantified by using the auto-threshold settings in Fiji/ImageJ software.[51]

Evaluation of mPTP opening

Hippocampal neurons (1×10^2 cells/well, DIV 14) plated onto Lab-Tek 4-well chamber slides were

treated with 1 μM Calcein Green AM (C3099, Thermo Fisher Scientific) or 1μM Calcein Red AM (C34851, Thermo Fisher Scientific) at 37°C for 30 min, then treated +/- 1 mM cobalt chloride ($CoCl_2$) for 30 min. Images were acquired at 37°C with a 40X oil-immersion objective (Neofluar, NA 1.3) on an epifluorescence microscope (Axio Observer Z1, Zeiss) with Colibri LED light source, EMCCD camera (Hamamatsu) and Zen 2012 (blue edition) software. Quantification of calcein fluorescence intensity was measured and quantified using the auto-threshold settings in Fiji/ImageJ software.

Immunofluorescence staining

Floating brain sections or fixed primary mouse neurons or cybrid cells were incubated overnight with the following primary antibodies: mouse anti-oligomeric Tau antibody TOMA-1 (1:2500, Millipore sigma, MABN819), rabbit polyclonal anti-oligomeric Tau antibody T22 (1:2500, ABN454; Millipore), mouse anti-Synapsin I antibody (1:1000, 611393, BD Biosciences), mouse anti-phospho-Tau pSer202/Thr205 (1:1000, MN1020, ThermoFisher Scientifc), rabbit anti-phospho-Tau pSer202/Thr205 (1:1000, 30505, Cell Signaling), and chicken MAP2 (1:5000, ab5392, Abcam). They were then incubated for 1 h with secondary antibodies (Alexa Fluor® 488, 594, and 633 goat anti-rabbit or anti-mouse IgG, 1:2000 dilution). Coverslips were mounted with VectaShield (Vector Laboratories) and sealed with clear nail polish. Images were acquired with a 63X objective (Neofluar, NA 1.4) on a Zeiss LSM 800 confocal microscope running Zen2 software. The images were manually measured and quantified using the auto-threshold settings in Fiji/ImageJ software. In **Supplementary Fig. S2A,** far-red fluorescence has been changed to white for clearer visualization.

Quantitative real-time PCR

Total RNA was extracted from hippocampal neurons using Trizol, as previously described.[52] 1 μg RNA was processed directly to produce cDNA using Reserve Transcription Supermix for RT-qPCR (#1708841, Bio-rad). Real-time PCR was utilized for quantification of mRNA expression of CypD (qMmuCID0008663, Bio-rad) and GAPDH (315637588, Integrated DNA technologies). Quantitative real-time PCR was performed by using CFX96 Real-Time System machine (Bio-rad).

Data were calculated using the 2 - $^{\Delta\Delta}$Ct method, as described by the manufacturer, and expressed as fold increase over the indicated controls (1.0) in each figure.

Statistical Analyses

Graphing and statistics were performed using GraphPad Prism (Version 9.4.0). Unpaired, two-tailed t-tests were used for pairwise comparison; one-way or two-way ANOVA with Fisher's least significant difference (LSD) tests were used for multiple comparisons. Data points and column data are depicted as mean ± standard deviation as described in corresponding figure legends. Statistical significance was obtained when $P < 0.05$. Individual *P*-values are indicated on graphs, and *n* numbers are indicated in the corresponding figure legends. Investigators were blinded to treatment conditions when performing analyses for all experiments.

Data availability

The data generated and analyzed in this study are available from the corresponding author upon reasonable request.

Results

GCs induce Tau pathology and mitochondrial dysfunction in hippocampus

To mimic chronic stress-induced GC release, we administered the synthetic GC dexamethasone (DEX; 5 mg/kg) to 4-5-month-old mice via intraperitoneal injection for 15 days, similar to previous studies[53-56]. DEX administration caused a ~10% loss of body weight and decreased endogenous blood corticosterone levels by more than 60% compared to vehicle control (Supplementary Fig. 1A, B), demonstrating its ability to cross the blood brain barrier and promote an endocrine response to stress. Since chronic stress and high GC levels are known to induce Tau accumulation and phosphorylation,[7,14-17] we verified these effects by immunoblotting with

antibodies against total (Tau5) and phosphorylated (AT8, PHF1) Tau species. We observed a two- to three-fold increase in phospho-Tau levels and a nearly two-fold increase in total Tau following DEX treatment (Fig. 1A-D). GCs are also reported to damage neuronal mitochondria,[33,36] and we verified that DEX administration induced a significant increase in mitochondrial reactive oxygen species (mROS) and a concomitant decrease in mitochondrial membrane potential, as measured by staining with the cell-permeant dyes MitoSOX and TMRM, respectively (Fig. 1E-H). With the exception of weight loss, these pathogenic effects of DEX were attenuated by co-administration of the GR antagonist mifepristone (Supplementary Fig. 1, Fig. 1).

Considerable evidence indicates that pathogenic Tau promotes mitochondrial dysfunction and vice-versa;[21-26,31,32] thus, we next examined whether oligomeric Tau was detected in the vicinity of mROS following chronic GC exposure. Hippocampal slices were incubated with MitoSOX, then fixed and immunostained with TOMA-1 antibodies to label Tau oligomers. Both MitoSOX and TOMA-1 levels were dramatically elevated in neurons of DEX-treated animals compared to those treated with vehicle control or DEX + mifepristone (Fig. 2A-C), indicative of Tau pathogenesis and mitochondrial dysfunction. Moreover, we observed a high degree of colocalization between MitoSOX and TOMA-1 in these neurons (Fig. 2A, D), showing that Tau oligomers and mROS are spatially coupled. The effects of GCs on mitochondrial function were further evaluated by measuring the activity of complex I, the first component of the electron transport chain, and ATP production using commercial kits. DEX significantly impaired mitochondrial function by both measures, decreasing ATP production and complex I activity by 30~40% compared to control and DEX + mifepristone conditions (Fig. 2E, F). We observed similar effects in 14 day *in vitro* (DIV) cultured hippocampal neurons treated with vehicle or DEX (1 mM, 48 hrs), with Tau pathology measured by TOMA-1/AT8 immunostaining (Supplementary Fig. 2A-C), and mitochondrial dysfunction by MitoSOX (Supplementary Fig. 2A, D, E) and TMRM (Supplementary Fig. 2H, I).

GCs stimulate mPTP opening via upregulation of cyclophilin D

One event known to promote mitochondrial dysfunction is opening of the mitochondrial permeability transition pore (mPTP), a channel on the inner mitochondrial membrane whose

components include the F_1/F_0 ATP synthase and the mitochondrial matrix protein cyclophilin D (CypD).[29] mPTP opening is triggered by various cellular stressors and mediated by CypD binding to a subunit of the ATP synthase[29]. Both knockout/knockdown of CypD and inhibition of its activity via treatment with the drug cyclosporin A have been shown to prevent mPTP opening and protect cells against mitochondrial dysfunction.[57-62] We assessed the effect of GCs on mPTP opening in 14 DIV cultured hippocampal neurons treated with vehicle or DEX (1 μM, 48 hrs). Here, we utilized the Co^{2+}-calcein dye assay,[61] which takes advantage of the fact that $CoCl_2$ quenches calcein fluorescence in all subcellular compartments except for mitochondria, due to the Co^{2+}-impermeable inner mitochondrial membrane. However, upon mPTP opening, Co^{2+} enters the inner mitochondrial matrix and quenches calcein fluorescence. This effect is blocked by cyclosporin A, showing its dependence on CypD.[61] We observed no quenching of calcein fluorescence by $CoCl_2$ in control cells, but significant quenching (nearly 80%) in DEX-treated cells **(**Fig. 3A, B**),** indicative of mPTP opening. Concomitant treatment of neurons with cyclosporin A (1 mM, 24 hrs) or knockdown of CypD with siRNAs (Supplementary Fig. 2F, G) attenuated $CoCl_2$-mediated calcein quenching (Fig. 3A, B). Cyclosporin A and CypD knockdown also prevented DEX-induced mitochondrial dysfunction as measured by MitoSOX fluorescence intensity, complex I activity, and ATP production (Fig. 3C-F), as well as TMRM intensity (Supplementary Fig. 2H, I).

CypD expression is elevated in brain tissue from Alzheimer's disease patients and mouse models,[57,58] and CypD deficiency is protective against Alzheimer's-related neurodegeneration,[57] consistent with the concept that CypD levels and mPTP opening are correlated with neurotoxicity. GCs are known to regulate gene transcription via their activation of GRs, which translocate to the nucleus and bind glucocorticoid response elements (GREs) within the promoter regions of multiple genes.[63] We therefore tested whether CypD expression is regulated by GCs. First, we measured CypD protein levels in hippocampal tissue from animals administered vehicle control or DEX. Immunoblots revealed that CypD expression was two-fold higher in DEX-treated tissue compared to control (Fig. 3G, H). This effect was likely not due to GC-induced accumulation of mitochondria, as previously reported,[36] since mPTP component oligomycin sensitivity-conferring protein (OSCP) was decreased by 50% following DEX treatment, and the outer mitochondrial membrane protein TOM20 was unchanged (Fig. 2G-J). We next performed qPCR to measure CypD mRNA levels in 14 DIV hippocampal neurons treated with DEX or vehicle control. Again,

we observed that CypD mRNA was significantly elevated by DEX (Fig. 2K). Moreover, eleven GREs were identified within the mouse *Ppif* gene (encoding CypD) by the Gene Transcription Regulation Database (https://gtrd.biouml.org/#!)(Table 1), supporting the hypothesis that GCs regulate CypD expression.

Since oligomeric Tau is associated with damaged mitochondria (Fig. 2), we next tested whether inhibiting mPTP opening with cyclosporin A or CypD knockdown could prevent GC-induced Tau pathology. Following treatment with vehicle control or DEX +/- cyclosporin A or CypD siRNAs, 14 DIV hippocampal neurons were immunostained with AT8 and TOMA-1 antibodies to measure phosphorylated and oligomeric Tau, respectively. Remarkably, both cyclosporin A and CypD knockdown prevented the dramatic increases in AT8 and TOMA-1 levels induced by DEX (Fig. 4A-C). Similar results were seen by immunoblotting, as cyclosporin A and CypD knockdown mitigated the DEX-induced increase in total and phospho-Tau species (Fig. 4D-G). Together, these findings suggest that inhibiting mPTP opening is protective against GC-induced Tau pathology, and that Tau pathogenesis likely occurs downstream of mitochondrial dysfunction in this context.

Mito-apocynin protects against GC-induced mPTP opening, mitochondrial damage, and Tau pathology *in vitro*

Our experiments in cultured neurons suggest that inhibiting mPTP opening could be an effective strategy for preventing stress/GC-related brain pathology. Unfortunately, cyclosporin A and CypD siRNAs are not currently viable approaches for therapeutic use, as cyclosporin A is an immunosuppressant and cannot cross the blood brain barrier,[64,65] and CypD siRNAs require invasive delivery methods (*e.g.* virus or intrathecal injection). We therefore sought a therapeutic approach that would inhibit mPTP opening and be more clinically tractable. To this end, we tested mito-apocynin, a mitochondria-targeted inhibitor of NADPH oxidase that is orally bioavailable and has been shown to protect against mitochondria-related toxicity and neurodegeneration in mouse models.[66-69] We first investigated whether mito-apocynin prevented GC-induced mPTP opening in hippocampal neurons, using the Co^{2+}-calcein assay described above. Indeed, treatment of 14 DIV neurons with mito-apocynin (1 mM, 24 hrs) prevented Co^{2+} quenching of calcein fluorescence stimulated by DEX (Fig. 5A, B). Interestingly, mito-apocynin also attenuated the

DEX-driven upregulation of CypD expression (Fig. 5C, D), suggesting that it acts in part by inhibiting CypD-mediated mPTP opening. To confirm this mechanism, we overexpressed GFP-CypD in hippocampal neurons via lentiviral transduction, which increased its levels by approximately three-fold over endogenous CypD (Fig. 5C, D). Indeed, GFP-CypD overexpression blocked the protective effects of mito-apocynin on GC-induced mPTP opening (Fig. 5A, B). Treatment with mito-apocynin also attenuated GC-induced Tau oligomerization and mROS production (Fig. 5E-G), as well as the GC-induced suppression of complex I activity and ATP production (Fig. 5H, I). Again, GFP-CypD overexpression blocked these protective effects of mito-apocynin on Tau pathogenesis and mitochondrial function (Fig. 5E-I).

Mito-apocynin protects against GC-induced behavioral and cellular effects *in vivo*

We next tested whether mito-apocynin could protect against the detrimental effects of GC exposure *in vivo*. Here, 4-5-month-old mice were administered vehicle control, DEX, or DEX + mifepristone via intraperitoneal injection for 15 days, and concomitantly given mito-apocynin or its vehicle control by oral gavage. Animals treated with DEX or DEX + mito-apocynin displayed similar body weight loss, demonstrating comparable physiological responses to GCs (Supplementary Fig. 1A). While mito-apocynin slightly but significantly attenuated the ~60% decrease in endogenous blood corticosterone levels caused by DEX administration, it did not rescue these levels to the same extent as mifepristone (Supplementary Fig. 2), suggesting a different mode of action. Since stress and high GC levels are known to induce changes in cognition and mood, including impaired learning and memory, anxiety, and depression,[2,7] we measured these behaviors using the Y-maze, elevated plus maze (EPM), and forced swim test (FST), respectively. Mice administered DEX showed a 30% decrease in spontaneous alternations in the Y-maze compared to the control group (Fig. 6A), indicating deficits in spatial memory. Remarkably, mito-apocynin prevented this GC-induced learning/memory deficit and had similar efficacy to mifepristone (Fig. 6A). Total distance traveled in the maze was unchanged across the four groups (Fig. 6B), showing that none of the treatments altered the animals' overall activity levels. Animals administered DEX also spent 50% less time in the open arm (and 50% more time in the closed arm) of the EPM compared to controls (Fig. 6C, D), indicative of heightened anxiety. Mito-

apocynin also prevented this anxious behavior with similar efficacy as mifepristone (Fig. 6C, D). Finally, DEX-administered animals spent nearly twice as much time immobile during the FST as control animals (Fig. 6E), suggestive of depressive behavior. Once again, mito-apocynin ameliorated this phenotype as effectively as mifepristone (Fig. 6E), showing the mitochondrially-targeted compound's efficacy at preventing GC-induced behavioral impairment.

Consistent with their detrimental effects on learning and memory, GCs cause dendrite and synapse loss in areas CA1 and CA3 of the hippocampus.[7,54,70,71] Indeed, DEX administration led to significantly decreased dendrite and synapse density in area CA1 as revealed by immunostaining with MAP2 and Synapsin1 antibodies, respectively (Fig. 6F-H). Mito-apocynin prevented the GC-induced loss of dendrites and synapses to a similar extent as mifepristone (Fig. 6F-H), indicative of its neuroprotective effects. Precipitating events in stress/GC-driven synapse loss include the synaptic missorting of phosphorylated and oligomeric Tau species, as well as mitochondrial dysfunction.[7,8,36,63] Since mito-apocynin protects against GC-induced Tau pathology and mitochondrial damage *in vitro*, we next assessed this compound's ability to inhibit these effects *in vivo*. Here, levels of oligomeric Tau and mROS were measured in hippocampal tissue by TOMA-1 and MitoSOX staining. Again, mito-apocynin was as effective as mifepristone in preventing GC-driven Tau oligomerization and mROS formation (Fig. 6I-K), with equal efficacy in male and female animals (Supplementary Fig. 3A, B). Mito-apocynin also prevented Tau accumulation and phosphorylation, as shown by immunoblotting for Tau5, AT8, and PHF1 in tissue lysates (Supplementary Fig. 4A-D), as well as GC-driven mitochondrial dysfunction as assessed by TMRM fluorescence, complex 1 activity, and ATP production in hippocampal tissue (Supplementary Fig. 4E-H), indicating that its effects derive from prevention of GC-induced mitochondrial damage and Tau pathology.

Mifepristone and mito-apocynin mitigate Tau pathology in cybrid cells

Our studies indicate that mitochondrial dysfunction promotes Tau pathogenesis in a mouse model of chronic stress, and that both GC-induced processes can be rescued by mifepristone or mito-apocynin. To investigate whether these treatments are similarly effective at mitigating

mitochondrial damage and Tau pathology in a human disease model, we utilized SH-SY5Y cybrid cells, an *ex vivo* Alzheimer's disease model in which endogenous mitochondria have been replaced with platelet-derived mitochondria from Alzheimer's subjects and age-matched controls.[30] Alzheimer's mitochondria exhibit multiple deficits compared to control mitochondria (*e.g.* decreased ATP production, increased mROS production, depolarized membrane potential), and Alzheimer's cybrid cells recapitulate key changes observed in patient brains, including increased expression of markers of oxidative stress, inflammation, and apoptosis, as well as higher levels of oligomeric Tau.[30-32] Following treatment of staurosporine-differentiated cybrid cells with vehicle control, mifepristone or mito-apocynin, we assessed Tau pathology and mitochondrial function. Consistent with previous reports, we found that the differentiated Alzheimer's cybrid cells contained far more oligomeric and phosphorylated Tau than the differentiated control cells and exhibited a greater than three-fold increase in mROS (Fig. 7A-D). As in murine primary hippocampal neurons and brain tissue, Tau oligomers were highly colocalized with MitoSOX in Alzheimer's cybrids (Fig. 7A, E). Measurement of complex I activity and ATP production also revealed a nearly 40% decrease in mitochondrial function in Alzheimer's cybrid cells relative to control cells (Fig. 7F, G). Remarkably, all of the observed Tau and mitochondrial phenotypes in Alzheimer's cybrids were restored to the level of control cybrid cells by treatment with mifepristone or mito-apocynin (Fig. 7A-G). These findings implicate GR signaling and mPTP opening as drivers of Alzheimer's disease-related mitochondrial dysfunction, and show that this dysfunction drives Tau oligomerization in the context of both stress and Alzheimer's disease.

Discussion

Long-term GC exposure negatively impacts brain structure and function, causing dendrite and synapse loss as well as learning/memory impairment, anxiety, and anhedonia[2,63]. Here, we demonstrate that a key precipitating event for these phenotypes is mitochondrial dysfunction, which in turn promotes the formation of neurotoxic Tau species. While GCs have been shown to impair mitochondrial function through a variety of mechanisms,[33] we identify mPTP opening, via GC-mediated upregulation of CypD, as a critical mechanism in stress/GC-related brain pathology. Interestingly, mPTP opening and CypD also appear to play important roles in other forms of brain

injury and neurodegeneration.[72] mPTP opening is triggered by ROS production and/or disruption of Ca^{2+} homeostasis, both of which are associated with ischemia, inflammation, neurodegenerative disease, and physiological aging; pore opening initiates a positive feedback loop that further exacerbates cellular damage.[72] CypD, a mitochondrial matrix protein and component of the mPTP, is a key mediator of mPTP formation and opening. CypD is elevated in brain tissue from patients with Alzheimer's disease as well as mouse models of Alzheimer's disease and amyotrophic lateral sclerosis.[57,73] Moreover, CypD inhibition/ablation is protective against ischemia and neurodegeneration in mouse models of amyotrophic lateral sclerosis, Alzheimer's disease, and Parkinson's disease,[57-60,73] indicating its potential value as a therapeutic target.

Unfortunately, current inhibitors of CypD, including cyclosporin A and its derivatives, are clinically intractable due to neurotoxicity, low selectivity, and unfavorable pharmacokinetics.[62] While other small molecule CypD inhibitors are under development,[62] CypD-independent therapeutics that directly target mitochondria have shown some promise in preventing mPTP opening and slowing neurodegeneration in mice.[72] We therefore adopted this strategy in our studies by using mitochondrially-targeted apocynin, a plant derivative that inhibits NADPH oxidases,[74] membrane-bound enzymes that catalyze the production of superoxide and are one of the main cellular sources of ROS.[75] Pharmacokinetic studies report that orally administered mito-apocynin at concentrations between 3-30 mg/kg rapidly crosses the blood brain barrier (within 30 minutes) and persists in the brain for at least 48 hours.[66] Moreover, clinical pathology data indicates that this compound causes no adverse effects 48 hours post-administration,[66] and multiple studies have demonstrated the beneficial effects of chronic mito-apocynin administration in mouse models of Parkinson's disease and excitotoxic injury.[66-68]

An important and surprising finding from our work is that mito-apocynin prevents neuronal damage caused by GCs. By targeting ROS production within mitochondria, mito-apocynin inhibits GC-driven mPTP opening and downstream Tau phosphorylation and oligomerization, synapse loss, and behavioral deficits. It is possible that mito-apocynin also impacts other aspects of mitochondrial health and function that were not assessed in this study, including mitochondrial transport, fission/fusion, etc. Of note, another recent study showed that GCs impair neuronal mitophagy by downregulating the mitophagy adaptor protein BNIP3L/NIX[36], and it is possible that this effect is also mitigated by mito-apocynin. Moreover, since mitochondria synthesize steroid hormones,[76] it is conceivable that mito-apocynin prevents GC-induced damage by altering

mitochondrial GC production or responsiveness to fluctuating GC levels. Indeed, we find that mito-apocynin administration slightly but significantly attenuates the dex-induced suppression of endogenous plasma corticosterone levels (Supplementary Fig. 1B), similar to mifepristone (albeit to a much lesser extent; ~10% vs. ~40%). This finding suggests that mito-apocynin can impact circulating GC levels. However, multiple studies support this compound's ability to prevent mitochondrial damage in animal models of neurological disease,[66-68] indicating that its primary mode of action is mROS inhibition. Regardless of the specific mechanism, our findings clearly demonstrate that mito-apocynin's inhibition of mitochondrial damage protects neurons against chronic GC exposure.

Mito-apocynin may also exert its protective effects through non-neuronal cells. Indeed, astrocytes and microglia are activated by chronic stress and elevated GC levels, leading them to release pro-inflammatory cytokines that promote the recruitment of peripheral immune cells to the brain and stimulate neuroinflammation and downstream synapse/neuron loss.[77,78] An integral part of the glial inflammatory response is ROS production, which was found to be significantly elevated by chronic stress/GCs.[77] Interestingly, inhibition of microglial ROS production was shown to mitigate anxious behaviors in chronically stressed mice,[79] indicating that microglia-initiated oxidative damage contributes to the behavioral deficits induced by stress. Whether these ROS derive from mitochondria or other superoxide-producing enzymes in the microglial cytoplasm or other organelles, and in general how GC-induced mitochondrial dysfunction contributes to the stress responses of glia and other non-neuronal cells, are interesting questions for future studies.

Our work also demonstrates that GCs promote Tau oligomerization through mitochondria. Precisely how mitochondrial damage induces the formation of Tau oligomers remains an open question. Tau phosphorylation stimulates its oligomerization, and inhibiting mitochondrial function is reported to activate Tau kinases, likely via ROS production.[30,80] Two other studies show that cytochrome c leakage from damaged mitochondria activates caspase 3, leading to Tau cleavage and aggregation.[81,82] Whether these mechanisms are responsible for Tau pathology downstream of GC-driven mitochondrial dysfunction is an important question that will be addressed in our ongoing work.

Although our experiments indicate that Tau oligomerization occurs downstream of GC-induced mitochondrial dysfunction, it is also likely that pathogenic Tau stimulates mitochondrial damage

following GC exposure. Multiple studies show that Tau impacts mitochondrial dynamics and function,[21-26] and Tau was recently reported to interact with a series of mitochondrial proteins, including outer and inner mitochondrial membrane proteins and components of the electron transport chain.[83] Moreover, Tau deletion was shown to protect against stress/GC-induced brain pathology, including synaptic loss in the hippocampus and prefrontal cortex (PFC).[7,8] Proteomic and electron microscopy analyses of PFC synapses in wild-type and Tau knockout mice revealed one major difference between these genotypes: Tau knockout animals exhibited significantly increased mitochondrial density at synapses following exposure to chronic stress, while wild-type animals exhibited a trend toward decreased mitochondrial density.[8] This finding suggests that stress/GCs regulate mitochondrial localization at synapses in a Tau-dependent manner, and that mitochondrial loss contributes to stress/GC-induced synaptic dysfunction. Indeed, exposure to stress may create a vicious cycle wherein GC-induced mitochondrial dysfunction precipitates Tau pathology, which in turn promotes additional mitochondrial damage leading to synapse loss and other neurotoxic effects. Given the ability of therapeutic strategies targeting either Tau (*i.e.* [7,8,20]) or mitochondria (*i.e.* [36], the current study) to prevent stress/GC-induced brain pathology in rodents, it is evident that both are critical players in this process.

Finally, our work shows that GR signaling has relevance to mitochondrial damage and Tau pathogenesis in a cellular model of Alzheimer's disease. Specifically, we find that treatment of Alzheimer's cybrid cells with the GR antagonist mifepristone is able to restore multiple aspects of mitochondrial function (*i.e.* complex 1 activity, ATP production, mitochondrial membrane potential, mROS production) to the level of control cybrid cells. Mifepristone similarly prevents Tau pathology (phosphorylation and oligomerization) in these cells, which we and others[32] observe to be spatially and temporally coupled to mROS production. Since exogenous GCs were not added to the cells, it is unclear why mifepristone has these effects. One possibility is that Alzheimer's subject-derived mitochondria are particularly sensitive to GCs present at low levels in the culture medium, likely deriving from fetal bovine serum.[84] Another is that GC synthesis occurs in cybrid cells and is upregulated in Alzheimer's mitochondria, leading to high local GC levels that are toxic to the mitochondria. It is also conceivable that mifepristone, an anti-progestogen, acts on Alzheimer's cybrid cells by blocking the effects of progesterone, which like GCs can be a component of fetal bovine serum.[85] Additional experiments will be required to distinguish between these possibilities and better understand how mifepristone exerts its protective effects. However,

the ability of mito-apocynin to similarly rescue Tau phosphorylation and oligomerization in Alzheimer's cybrid cells suggests that mitochondria are a promising therapeutic target for preventing Tau pathogenesis.

In summary, we identify a novel molecular pathway by which GCs induce mitochondrial dysfunction, via transcriptional upregulation of the mPTP activating protein CypD. Further, we show that this mitochondrial damage precipitates Tau pathology. Our studies in both murine hippocampus and Alzheimer's cybrid cells not only link mitochondrial dysfunction to Tau pathology in the context of stress, but also indicate that mitochondrially-targeted therapeutics may be protective against Tau pathology associated with Alzheimer's disease.

Acknowledgements

We thank Irla Belli for subcloning and lentiviral production of GFP-CypD, Konner Kirwan for discussions about statistics, Mu Yang and Paul Hamblin (Columbia Mouse Neurobehavior Core) for help with behavioral experiments, and Ioannis Sotiropoulos and members of the Sotiropoulos lab for advice on behavioral testing and other helpful discussions about stress-related brain pathology. The GRE data used in this manuscript was obtained from the Gene Transcription Regulation Database (https://gtrd.biouml.org/#!) on 09/30/22.

Funding

This work was supported by NIH grants R01NS080967 and RF1AG069941 to C.L.W. and P30 AG072973 to R.H.S.

Competing interests

The authors report no competing interests.

Supplementary material

Supplementary material is available at *Brain* online.

References

1. McEwen BS. Stress-induced remodeling of hippocampal CA3 pyramidal neurons. *Brain Res*. Aug 15 2016;1645:50-4. doi:10.1016/j.brainres.2015.12.043

2. McEwen BS, Bowles NP, Gray JD, et al. Mechanisms of stress in the brain. *Nat Neurosci*. Oct 2015;18(10):1353-63. doi:10.1038/nn.4086

3. Machado A, Herrera AJ, de Pablos RM, et al. Chronic stress as a risk factor for Alzheimer's disease. *Rev Neurosci*. 2014;25(6):785-804. doi:10.1515/revneuro-2014-0035

4. Mravec B, Horvathova L, Padova A. Brain Under Stress and Alzheimer's Disease. *Cell Mol Neurobiol*. Jan 2018;38(1):73-84. doi:10.1007/s10571-017-0521-1

5. Cohen S, Janicki-Deverts D, Miller GE. Psychological stress and disease. *JAMA*. Oct 10 2007;298(14):1685-7. doi:10.1001/jama.298.14.1685

6. Sotiropoulos I, Silva JM, Gomes P, Sousa N, Almeida OFX. Stress and the Etiopathogenesis of Alzheimer's Disease and Depression. *Adv Exp Med Biol*. 2019;1184:241-257. doi:10.1007/978-981-32-9358-8_20

7. Lopes S, Vaz-Silva J, Pinto V, et al. Tau protein is essential for stress-induced brain pathology. *Proc Natl Acad Sci U S A*. Jun 28 2016;113(26):E3755-63. doi:10.1073/pnas.1600953113

8. Lopes S, Teplytska L, Vaz-Silva J, et al. Tau Deletion Prevents Stress-Induced Dendritic Atrophy in Prefrontal Cortex: Role of Synaptic Mitochondria. *Cereb Cortex*. Apr 1 2017;27(4):2580-2591. doi:10.1093/cercor/bhw057

9. Holper S, Watson R, Yassi N. Tau as a Biomarker of Neurodegeneration. *International journal of molecular sciences*. Jun 30 2022;23(13)doi:10.3390/ijms23137307

10. Shively SB, Priemer DS, Stein MB, Perl DP. Pathophysiology of Traumatic Brain Injury, Chronic Traumatic Encephalopathy, and Neuropsychiatric Clinical Expression. *Psychiatr Clin North Am*. Sep 2021;44(3):443-458. doi:10.1016/j.psc.2021.04.003

11. Fyfe I. Epilepsy: Tau pathology found in temporal lobe epilepsy. *Nat Rev Neurol*. Oct 2016;12(10):554. doi:10.1038/nrneurol.2016.130

12. Niewiadomska G, Niewiadomski W, Steczkowska M, Gasiorowska A. Tau Oligomers Neurotoxicity. *Life (Basel)*. Jan 6 2021;11(1)doi:10.3390/life11010028

13. Brunden KR, Trojanowski JQ, Lee VM. Evidence that non-fibrillar tau causes pathology linked to neurodegeneration and behavioral impairments. *J Alzheimers Dis*. Aug 2008;14(4):393-9. doi:10.3233/jad-2008-14406

14. Yi JH, Brown C, Whitehead G, et al. Glucocorticoids activate a synapse weakening pathway culminating in tau phosphorylation in the hippocampus. *Pharmacol Res*. Jul 2017;121:42-51. doi:10.1016/j.phrs.2017.04.015

15. Dey A, Hao S, Wosiski-Kuhn M, Stranahan AM. Glucocorticoid-mediated activation of GSK3beta promotes tau phosphorylation and impairs memory in type 2 diabetes. *Neurobiol Aging*. Sep 2017;57:75-83. doi:10.1016/j.neurobiolaging.2017.05.010

16. Sotiropoulos I, Catania C, Riedemann T, et al. Glucocorticoids trigger Alzheimer disease-like pathobiochemistry in rat neuronal cells expressing human tau. *J Neurochem*. Oct 2008;107(2):385-97. doi:10.1111/j.1471-4159.2008.05613.x

17. Sotiropoulos I, Catania C, Pinto LG, et al. Stress acts cumulatively to precipitate Alzheimer's disease-like tau pathology and cognitive deficits. *J Neurosci*. May 25 2011;31(21):7840-7. doi:10.1523/JNEUROSCI.0730-11.2011

18. Sotiropoulos I, Silva J, Kimura T, et al. Female hippocampus vulnerability to environmental stress, a precipitating factor in Tau aggregation pathology. *J Alzheimers Dis*. 2015;43(3):763-74. doi:10.3233/JAD-140693

19. Silva JM, Rodrigues S, Sampaio-Marques B, et al. Dysregulation of autophagy and stress granule-related proteins in stress-driven Tau pathology. *Cell Death Differ*. Nov 15 2018;doi:10.1038/s41418-018-0217-1

20. Vaz-Silva J, Gomes P, Jin Q, et al. Endolysosomal degradation of Tau and its role in glucocorticoid-driven hippocampal malfunction. *EMBO J*. Aug 30 2018;doi:10.15252/embj.201899084

21. Lasagna-Reeves CA, Castillo-Carranza DL, Sengupta U, Clos AL, Jackson GR, Kayed R. Tau oligomers impair memory and induce synaptic and mitochondrial dysfunction in wild-type mice. *Molecular neurodegeneration*. Jun 6 2011;6:39. doi:10.1186/1750-1326-6-39

22. Camilleri A, Ghio S, Caruana M, et al. Tau-induced mitochondrial membrane perturbation is dependent upon cardiolipin. *Biochim Biophys Acta Biomembr*. Feb 1 2020;1862(2):183064. doi:10.1016/j.bbamem.2019.183064

23. Zheng J, Akbari M, Schirmer C, et al. Hippocampal tau oligomerization early in tau pathology coincides with a transient alteration of mitochondrial homeostasis and DNA repair in a mouse model of tauopathy. *Acta Neuropathol Commun*. Mar 4 2020;8(1):25. doi:10.1186/s40478-020-00896-8

24. Manczak M, Reddy PH. Abnormal interaction between the mitochondrial fission protein Drp1 and hyperphosphorylated tau in Alzheimer's disease neurons: implications for mitochondrial dysfunction and neuronal damage. *Hum Mol Genet*. Jun 1 2012;21(11):2538-47. doi:10.1093/hmg/dds072

25. Schulz KL, Eckert A, Rhein V, et al. A new link to mitochondrial impairment in tauopathies. *Mol Neurobiol*. Aug 2012;46(1):205-16. doi:10.1007/s12035-012-8308-3

26. Perez MJ, Jara C, Quintanilla RA. Contribution of Tau Pathology to Mitochondrial Impairment in Neurodegeneration. *Front Neurosci*. 2018;12:441. doi:10.3389/fnins.2018.00441

27. Amadoro G, Corsetti V, Atlante A, et al. Interaction between NH(2)-tau fragment and Abeta in Alzheimer's disease mitochondria contributes to the synaptic deterioration. *Neurobiol Aging*. Apr 2012;33(4):833 e1-25. doi:10.1016/j.neurobiolaging.2011.08.001

28. Jara C, Aranguiz A, Cerpa W, Tapia-Rojas C, Quintanilla RA. Genetic ablation of tau improves mitochondrial function and cognitive abilities in the hippocampus. *Redox Biol*. Sep 2018;18:279-294. doi:10.1016/j.redox.2018.07.010

29. Bonora M, Giorgi C, Pinton P. Molecular mechanisms and consequences of mitochondrial permeability transition. *Nat Rev Mol Cell Biol*. Apr 2022;23(4):266-285.

doi:10.1038/s41580-021-00433-y

30. Swerdlow RH, Koppel S, Weidling I, Hayley C, Ji Y, Wilkins HM. Mitochondria, Cybrids, Aging, and Alzheimer's Disease. *Prog Mol Biol Transl Sci*. 2017;146:259-302. doi:10.1016/bs.pmbts.2016.12.017

31. Weidling IW, Swerdlow RH. Mitochondria in Alzheimer's disease and their potential role in Alzheimer's proteostasis. *Exp Neurol*. Aug 2020;330:113321. doi:10.1016/j.expneurol.2020.113321

32. Du F, Yu Q, Kanaan NM, Yan SS. Mitochondrial oxidative stress contributes to the pathological aggregation and accumulation of tau oligomers in Alzheimer's disease. *Hum Mol Genet*. Aug 17 2022;31(15):2498-2507. doi:10.1093/hmg/ddab363

33. Choi GE, Han HJ. Glucocorticoid impairs mitochondrial quality control in neurons. *Neurobiol Dis*. May 2021;152:105301. doi:10.1016/j.nbd.2021.105301

34. Picard M, McEwen BS, Epel ES, Sandi C. An energetic view of stress: Focus on mitochondria. *Front Neuroendocrinol*. Apr 2018;49:72-85. doi:10.1016/j.yfrne.2018.01.001

35. Du J, Wang Y, Hunter R, et al. Dynamic regulation of mitochondrial function by glucocorticoids. *Proc Natl Acad Sci U S A*. Mar 3 2009;106(9):3543-8. doi:10.1073/pnas.0812671106

36. Choi GE, Lee HJ, Chae CW, et al. BNIP3L/NIX-mediated mitophagy protects against glucocorticoid-induced synapse defects. *Nature communications*. Jan 20 2021;12(1):487. doi:10.1038/s41467-020-20679-y

37. Komada M, Takao K, Miyakawa T. Elevated plus maze for mice. *J Vis Exp*. Dec 22 2008;(22)doi:10.3791/1088

38. Kraeuter AK, Guest PC, Sarnyai Z. The Y-Maze for Assessment of Spatial Working and Reference Memory in Mice. *Methods Mol Biol*. 2019;1916:105-111. doi:10.1007/978-1-4939-8994-2_10

39. Yankelevitch-Yahav R, Franko M, Huly A, Doron R. The Forced Swim Test as a Model of Depressive-like Behavior. *Jove-J Vis Exp*. Mar 2015;(97)doi:ARTN e52587 10.3791/52587

40. Du F, Yu Q, Yan S, et al. PINK1 signalling rescues amyloid pathology and mitochondrial dysfunction in Alzheimer's disease. *Brain*. Dec 1 2017;140(12):3233-3251. doi:10.1093/brain/awx258

41. Miller SW, Trimmer PA, Parker WD, Jr., Davis RE. Creation and characterization of mitochondrial DNA-depleted cell lines with "neuronal-like" properties. *Journal of neurochemistry*. Nov 1996;67(5):1897-907.

42. Swerdlow RH. Mitochondria in cybrids containing mtDNA from persons with mitochondriopathies. *Journal of neuroscience research*. Nov 15 2007;85(15):3416-28. doi:10.1002/jnr.21167

43. Albert MS, DeKosky ST, Dickson D, et al. The diagnosis of mild cognitive impairment due to Alzheimer's disease: recommendations from the National Institute on Aging-Alzheimer's Association workgroups on diagnostic guidelines for Alzheimer's disease. *Alzheimer's & dementia : the journal of the Alzheimer's Association*. May 2011;7(3):270-9. doi:10.1016/j.jalz.2011.03.008

44. Yu Q, Du F, Douglas JT, Yu H, Yan SS, Yan SF. Mitochondrial Dysfunction Triggers Synaptic Deficits via Activation of p38 MAP Kinase Signaling in Differentiated Alzheimer's Disease Trans-Mitochondrial Cybrid Cells. *J Alzheimers Dis*. 2017;59(1):223-239. doi:10.3233/JAD-170283

45. Yu Q, Fang D, Swerdlow RH, Yu H, Chen JX, Yan SS. Antioxidants Rescue Mitochondrial Transport in Differentiated Alzheimer's Disease Trans-Mitochondrial Cybrid Cells. *J Alzheimers Dis*. Sep 6 2016;54(2):679-90. doi:10.3233/JAD-160532

46. Du F, Yu Q, Yan SS. PINK1 Activation Attenuates Impaired Neuronal-Like Differentiation and Synaptogenesis and Mitochondrial Dysfunction in Alzheimer's Disease Trans-Mitochondrial Cybrid Cells. *J Alzheimers Dis*. May 14 2021;doi:10.3233/JAD-210095

47. Du F, Yu Q, Yan SS. PINK1 Activation Attenuates Impaired Neuronal-Like Differentiation and Synaptogenesis and Mitochondrial Dysfunction in Alzheimer's Disease Trans-Mitochondrial Cybrid Cells. *J Alzheimers Dis*. 2021;81(4):1749-1761. doi:10.3233/JAD-210095

48. Prince JA, Oreland L. Staurosporine differentiated human SH-SY5Y neuroblastoma

cultures exhibit transient apoptosis and trophic factor independence. Comparative Study Research Support, Non-U.S. Gov't. *Brain research bulletin*. 1997;43(6):515-23.

49. Sheehan P, Zhu M, Beskow A, Vollmer C, Waites CL. Activity-Dependent Degradation of Synaptic Vesicle Proteins Requires Rab35 and the ESCRT Pathway. *J Neurosci*. Aug 17 2016;36(33):8668-86. doi:10.1523/JNEUROSCI.0725-16.2016

50. Birdsall V, Martinez JC, Randolph L, Hengst U, Waites CL. Live Imaging of ESCRT Proteins in Microfluidically Isolated Hippocampal Axons. *Methods Mol Biol*. 2019;1998:117-128. doi:10.1007/978-1-4939-9492-2_9

51. Fang D, Wang Y, Zhang Z, et al. Increased neuronal PreP activity reduces Abeta accumulation, attenuates neuroinflammation and improves mitochondrial and synaptic function in Alzheimer disease's mouse model. *Human molecular genetics*. Sep 15 2015;24(18):5198-210. doi:10.1093/hmg/ddv241

52. Rio DC, Ares M, Jr., Hannon GJ, Nilsen TW. Purification of RNA using TRIzol (TRI reagent). *Cold Spring Harb Protoc*. Jun 2010;2010(6):pdb prot5439. doi:10.1101/pdb.prot5439

53. Green KN, Billings LM, Roozendaal B, McGaugh JL, LaFerla FM. Glucocorticoids increase amyloid-beta and tau pathology in a mouse model of Alzheimer's disease. *J Neurosci*. Aug 30 2006;26(35):9047-56. doi:10.1523/JNEUROSCI.2797-06.2006

54. Pedrazzoli M, Losurdo M, Paolone G, et al. Glucocorticoid receptors modulate dendritic spine plasticity and microglia activity in an animal model of Alzheimer's disease. *Neurobiol Dis*. Dec 2019;132:104568. doi:10.1016/j.nbd.2019.104568

55. Skupio U, Tertil M, Sikora M, Golda S, Wawrzczak-Bargiela A, Przewlocki R. Behavioral and molecular alterations in mice resulting from chronic treatment with dexamethasone: relevance to depression. *Neuroscience*. Feb 12 2015;286:141-50. doi:10.1016/j.neuroscience.2014.11.035

56. Li WZ, Li WP, Yao YY, et al. Glucocorticoids increase impairments in learning and memory due to elevated amyloid precursor protein expression and neuronal apoptosis in 12-month old mice. *Eur J Pharmacol*. Feb 25 2010;628(1-3):108-15. doi:10.1016/j.ejphar.2009.11.045

57. Du H, Guo L, Fang F, et al. Cyclophilin D deficiency attenuates mitochondrial and neuronal perturbation and ameliorates learning and memory in Alzheimer's disease. *Nat Med*. Oct 2008;14(10):1097-105. doi:10.1038/nm.1868

58. Du H, Guo L, Zhang W, Rydzewska M, Yan S. Cyclophilin D deficiency improves mitochondrial function and learning/memory in aging Alzheimer disease mouse model. *Neurobiol Aging*. Mar 2011;32(3):398-406. doi:10.1016/j.neurobiolaging.2009.03.003

59. Sun J, Jacobs KM. Knockout of Cyclophilin-D Provides Partial Amelioration of Intrinsic and Synaptic Properties Altered by Mild Traumatic Brain Injury. *Front Syst Neurosci*. 2016;10:63. doi:10.3389/fnsys.2016.00063

60. Martin LJ, Semenkow S, Hanaford A, Wong M. Mitochondrial permeability transition pore regulates Parkinson's disease development in mutant alpha-synuclein transgenic mice. *Neurobiol Aging*. May 2014;35(5):1132-52. doi:10.1016/j.neurobiolaging.2013.11.008

61. Bonora M, Morganti C, Morciano G, Giorgi C, Wieckowski MR, Pinton P. Comprehensive analysis of mitochondrial permeability transition pore activity in living cells using fluorescence-imaging-based techniques. *Nat Protoc*. Jun 2016;11(6):1067-80. doi:10.1038/nprot.2016.064

62. Haleckova A, Benek O, Zemanova L, Dolezal R, Musilek K. Small-molecule inhibitors of cyclophilin D as potential therapeutics in mitochondria-related diseases. *Med Res Rev*. Sep 2022;42(5):1822-1855. doi:10.1002/med.21892

63. Vyas S, Rodrigues AJ, Silva JM, et al. Chronic Stress and Glucocorticoids: From Neuronal Plasticity to Neurodegeneration. *Neural plasticity*. 2016;2016:6391686. doi:10.1155/2016/6391686

64. Rao VK, Carlson EA, Yan SS. Mitochondrial permeability transition pore is a potential drug target for neurodegeneration. *Biochim Biophys Acta*. Aug 2014;1842(8):1267-72. doi:10.1016/j.bbadis.2013.09.003

65. Bellwon P, Culot M, Wilmes A, et al. Cyclosporine A kinetics in brain cell cultures and its potential of crossing the blood-brain barrier. *Toxicol In Vitro*. Dec 25 2015;30(1 Pt A):166-75. doi:10.1016/j.tiv.2015.01.003

66. Langley M, Ghosh A, Charli A, et al. Mito-Apocynin Prevents Mitochondrial

Dysfunction, Microglial Activation, Oxidative Damage, and Progressive Neurodegeneration in MitoPark Transgenic Mice. *Antioxid Redox Signal*. Nov 10 2017;27(14):1048-1066. doi:10.1089/ars.2016.6905

67. Liu N, Lin MM, Huang SS, et al. NADPH and Mito-Apocynin Treatment Protects Against KA-Induced Excitotoxic Injury Through Autophagy Pathway. *Front Cell Dev Biol*. 2021;9:612554. doi:10.3389/fcell.2021.612554

68. Ghosh A, Langley MR, Harischandra DS, et al. Mitoapocynin Treatment Protects Against Neuroinflammation and Dopaminergic Neurodegeneration in a Preclinical Animal Model of Parkinson's Disease. *J Neuroimmune Pharmacol*. Jun 2016;11(2):259-78. doi:10.1007/s11481-016-9650-4

69. Dranka BP, Gifford A, McAllister D, et al. A novel mitochondrially-targeted apocynin derivative prevents hyposmia and loss of motor function in the leucine-rich repeat kinase 2 (LRRK2(R1441G)) transgenic mouse model of Parkinson's disease. *Neurosci Lett*. Nov 7 2014;583:159-64. doi:10.1016/j.neulet.2014.09.042

70. McEwen BS. Stress and hippocampal plasticity. *Annu Rev Neurosci*. 1999;22:105-22. doi:10.1146/annurev.neuro.22.1.105

71. Liston C, Gan WB. Glucocorticoids are critical regulators of dendritic spine development and plasticity in vivo. *Proc Natl Acad Sci U S A*. Sep 20 2011;108(38):16074-9. doi:10.1073/pnas.1110444108

72. Kent AC, El Baradie KBY, Hamrick MW. Targeting the Mitochondrial Permeability Transition Pore to Prevent Age-Associated Cell Damage and Neurodegeneration. *Oxid Med Cell Longev*. 2021;2021:6626484. doi:10.1155/2021/6626484

73. Xiao Y, Karam C, Yi J, et al. ROS-related mitochondrial dysfunction in skeletal muscle of an ALS mouse model during the disease progression. *Pharmacol Res*. Dec 2018;138:25-36. doi:10.1016/j.phrs.2018.09.008

74. Li N, Zhang G, Yi FX, Zou AP, Li PL. Activation of NAD(P)H oxidase by outward movements of H+ ions in renal medullary thick ascending limb of Henle. *Am J Physiol Renal Physiol*. Nov 2005;289(5):F1048-56. doi:10.1152/ajprenal.00416.2004

75. Sahoo S, Meijles DN, Pagano PJ. NADPH oxidases: key modulators in aging and age-

related cardiovascular diseases? *Clin Sci (Lond)*. Mar 2016;130(5):317-35. doi:10.1042/CS20150087

76. Timmermans S, Souffriau J, Libert C. A General Introduction to Glucocorticoid Biology. *Front Immunol*. 2019;10:1545. doi:10.3389/fimmu.2019.01545

77. Picard K, St-Pierre MK, Vecchiarelli HA, Bordeleau M, Tremblay ME. Neuroendocrine, neuroinflammatory and pathological outcomes of chronic stress: A story of microglial remodeling. *Neurochem Int*. May 2021;145:104987. doi:10.1016/j.neuint.2021.104987

78. Dolotov OV, Inozemtseva LS, Myasoedov NF, Grivennikov IA. Stress-Induced Depression and Alzheimer's Disease: Focus on Astrocytes. *International journal of molecular sciences*. Apr 30 2022;23(9)doi:10.3390/ijms23094999

79. Lv H, Zhu C, Wu R, et al. Chronic mild stress induced anxiety-like behaviors can Be attenuated by inhibition of NOX2-derived oxidative stress. *J Psychiatr Res*. Jul 2019;114:55-66. doi:10.1016/j.jpsychires.2019.04.008

80. Yamada ES, Respondek G, Mussner S, et al. Annonacin, a natural lipophilic mitochondrial complex I inhibitor, increases phosphorylation of tau in the brain of FTDP-17 transgenic mice. *Exp Neurol*. Mar 2014;253:113-25. doi:10.1016/j.expneurol.2013.12.017

81. Zhao Y, Tseng IC, Heyser CJ, et al. Appoptosin-Mediated Caspase Cleavage of Tau Contributes to Progressive Supranuclear Palsy Pathogenesis. *Neuron*. Sep 2 2015;87(5):963-75. doi:10.1016/j.neuron.2015.08.020

82. Zhang H, Zhang YW, Chen Y, et al. Appoptosin is a novel pro-apoptotic protein and mediates cell death in neurodegeneration. *J Neurosci*. Oct 31 2012;32(44):15565-76. doi:10.1523/JNEUROSCI.3668-12.2012

83. Tracy TE, Madero-Perez J, Swaney DL, et al. Tau interactome maps synaptic and mitochondrial processes associated with neurodegeneration. *Cell*. Feb 17 2022;185(4):712-728 e14. doi:10.1016/j.cell.2021.12.041

84. Conover CA, Rosenfeld RG, Hintz RL. Serum glucocorticoids have persistent and controlling effects on insulinlike growth factor I action under serum-free assay conditions in cultured human fibroblasts. *In Vitro Cell Dev Biol*. Jun 1989;25(6):521-7. doi:10.1007/BF02623564

85. Milo GE, Malarkey WB, Powell JE, Blakeslee JR, Yohn DS. Effects of steroid hormones in fetal bovine serum on plating ang cloning of human cells in vitro. *In Vitro*. Jan 1976;12(1):23-30. doi:10.1007/BF02832789

Figure Legends

Figure 1 Dexamethasone induces Tau pathology and mitochondrial dysfunction *in vivo*. (**A-D**) Representative immunoblots (**A**) and quantification **(B-D)** of AT8, PHF1, and total Tau (Tau5) immunoreactivity in lysates from hippocampal tissue of mice treated with vehicle (CON), dexamethasone (DEX), or DEX + GR antagonist mifepristone (MIF). Intensity values are expressed relative to tubulin and normalized to the CON condition, (standard deviations and *P*-values indicated on graphs; one-way ANOVA with multiple comparisons and Fisher's LSD test; *n*=3 mice/condition). (**E-F**) Representative images (**E**) and quantification (**F**) of MitoSOX fluorescence intensity (green) in hippocampal area CA1 from mice treated as indicated. MitoTracker (green) shows mitochondrial distribution. Yellow boxes indicate enlarged regions (right column). Scale bars, 25 µm. Intensity values are normalized to DEX condition (standard deviations and *P*-values indicated on graph; one-way ANOVA with multiple comparisons and Fisher's LSD test; *n*=5-6 fields of view/condition). (**G-H**) Representative images (**G**) and quantification (**H**) of TMRM fluorescence intensity (red) in hippocampal area CA1 from mice treated as indicated. Nuclei are stained with DAPI. Scale bar, 50 µm. Intensity values are normalized to CON condition (standard deviations and *P*-values indicated on graph; one-way ANOVA with multiple comparisons and Fisher's LSD test; *n*=5 fields of view/condition).

Figure 2 Tau oligomerization and mitochondrial dysfunction are spatially coupled. (**A-C**) Representative images (**A**) and quantification (**B-C**) of TOMA-1 (green) and MitoSOX (red) fluorescence intensity in slices from hippocampal area CA1 of mice treated with vehicle (CON), DEX, or DEX + MIF. Yellow boxes indicate enlarged regions (bottom row). Size bars, 50 µm. Intensity values are normalized to control condition (standard deviations and *P*-values indicated on graphs; one-way ANOVA with multiple comparisons and Fisher's LSD test; *n*=5 mice per condition for **B**, *n*=4 mice per condition with two fields of view/animal for **C**). (**D)** Area of TOMA-

1 colocalization with MitoSOX, normalized to DEX condition due to the absence of TOMA-1 and MitoSOX staining in CON condition (standard deviations and *P*-values indicated on graph; one-way ANOVA with multiple comparisons and Fisher's LSD test; *n*=5 mice per condition with two fields of view/animal). (**E-F**) Complex I activity (**E**) and ATP levels (**F**) in hippocampal tissue from mice treated as indicated, normalized to CON condition (standard deviations and *P*-values indicated on graphs; one-way ANOVA with multiple comparisons and Fisher's LSD test; *n*=3-6 mice per condition for **E**, one-way ANOVA with multiple comparisons and Fisher's LSD test; *n*=3-4 mice per condition for **F**).

Figure 3 GCs stimulate mPTP opening and cyclophilin D expression. (**A-B**) Representative images (**A**) and quantification (**B**) of calcein green fluorescence intensity with or without $CoCl_2$ in hippocampal neurons treated with vehicle (CON), DEX, DEX + cyclosporin A (CsA), or DEX + siRNAs against Cyclophilin D (CypD KD). Scale bar, 25 μm. Intensity values are normalized to CON condition (standard deviations and *P*-values indicated on graph; 2-way ANOVA with multiple comparisons and Fisher's LSD test; *n*=10 fields of view/condition). (**C-D**) Representative images (**C)** and quantification (**D**) of MitoSOX fluorescence intensity (red) in cultured hippocampal neurons treated as indicated. MitoTracker (green) staining shows distribution of mitochondria. Yellow boxes indicate enlarged regions (right column). Scale bars, 25 μm. Intensity values are normalized to CON condition (standard deviations and *P*-values indicated on graph; one-way ANOVA with multiple comparisons and Fisher's LSD test; *n*=10 fields of view/condition). (**E-F**) Complex I activity (**E**) and ATP levels (**F**) in hippocampal neurons treated as indicated, normalized to CON condition (standard deviations and *P*-values indicated on graphs; one-way ANOVA with multiple comparisons and Fisher's LSD test; *n*=3-7 samples/condition for **E**; one-way ANOVA with multiple comparisons and Fisher's LSD test; *n*=3-7 samples/condition for **F**). (**G-J**) Representative immunoblots (**G**) and quantification **(H-J)** of CypD, oligomycin sensitivity-conferring protein (OSCP), and TOM20 immunoreactivity in lysates from cultured hippocampal neurons treated as indicated. Intensity values are expressed relative to tubulin and normalized to the CON condition (standard deviations and *P*-values indicated on graphs; unpaired t test, *n*=4 samples/condition). (**K**) Quantification of CypD mRNA levels in cultured hippocampal neurons treated as indicated. Values are normalized to CON condition (standard deviations and *P*-value indicated on graph; unpaired t-test, *n*=6 samples/condition, two independent cultures).

Figure 4 Inhibiting the mPTP prevents GC-induced Tau pathology. (**A-C**) Representative images (**A**) and quantification (**B-C**) of TOMA-1 (green) and AT8 (red) fluorescence intensity in MAP2 positive (grey) cultured hippocampal neurons treated with vehicle (CON), DEX, CsA, or CypD siRNAs (CypD KD). Yellow boxes indicate enlarged regions (right column). Scale bars, 25 µm. Intensity values are normalized to DEX condition (standard deviations and *P*-values indicated on graphs; one-way ANOVA with multiple comparisons and Fisher's LSD test; *n*=10 fields of views/condition). (**D-F**) Representative immunoblots (**D**) and quantifications (**E-F**) of AT8, PHF1, and total Tau (Tau5) immunoreactivity in lysates from cultured hippocampal neurons treated as indicated. Intensity values are expressed relative to tubulin and normalized to the CON condition (standard deviations and *P*-values indicated on graphs; one-way ANOVA with multiple comparisons and Fisher's LSD test; *n*=3 samples/condition).

Figure 5 Mito-apocynin prevents GC-induced mPTP opening, mitochondrial damage, and Tau pathology *in vitro.* (**A-B**) Representative images (**A**) and quantification (**B**) of calcein red fluorescence intensity with or without $CoCl_2$ in hippocampal neurons expressing GFP or GFP-CypD (green), treated with vehicle (CON), DEX, or DEX + mito-apocynin (mAPO). Scale bar, 25 µm. Intensity values are normalized to CON condition (standard deviations and *P*-values indicated on graph; 2-way ANOVA with multiple comparisons and Fisher's LSD test; *n*=10 fields of views/condition). (**C-D**) Representative immunoblots (**C**) and quantification (**D**) of CypD expression in lysates of cultured hippocampal neurons treated as indicated, with or without GFP-CypD lentiviral transduction. Values are expressed relative to tubulin and normalized to CON condition (standard deviations and *P*-values indicated on graph; one-way ANOVA with multiple comparisons and Fisher's LSD test; *n*=3 samples/condition). (**E-H**) Representative images (**E**) and quantification (**F-G**) of TOMA-1 (grey) and MitoSOX (red) fluorescence intensity in hippocampal neurons expressing GFP or GFP-CypD and treated as indicated. Yellow boxes indicate enlarged regions (right column). Scale bars, 25 µm. Values are normalized to DEX condition (standard deviations and *P*-values indicated on graphs; one-way ANOVA with multiple comparisons and Fisher's LSD test; *n*=8 fields of view/condition). (**H-I**) Complex I activity (**H**) and ATP levels (**I**) in hippocampal neurons treated as indicated, normalized to CON condition (standard deviations

and *P*-values indicated on graphs; one-way ANOVA with multiple comparisons and Fisher's LSD test; *n*=3-4 samples/condition).

Figure 6 Mito-apocynin prevents GC-induced behavioral deficits, synapse loss, and Tau pathology *in vivo*. (**A-B**) Y-maze spontaneous alternations (**A**), expressed as percent of total arm entries that alternated, and total distance traveled (**B**) for mice treated with vehicle (CON), DEX, DEX + MIF, or DEX + mAPO (standard deviations and *P*-values indicated on graphs; one-way ANOVA with multiple comparisons and Fisher's LSD test; *n*=4-5 mice/condition). (**C-D**) Time spent in open (**C**) and closed (**D**) arms of EPM for mice treated as indicated (standard deviations and *P*-values indicated on graphs; one-way ANOVA with multiple comparisons and Fisher's LSD test; *n*=9-10 mice/condition). (**E**) Time spent immobile during FST for mice treated as indicated (standard deviations and *P*-values indicated on graph; one-way ANOVA with multiple comparisons and Fisher's LSD test; *n*=9-10 mice/condition). (**F-H**) Representative images (**F**) and quantification (**G, H**) of Synapsin1 (green) and MAP2 (purple) immunofluorescence intensity in hippocampal area CA1 from mice treated as indicated. Nuclei are stained by DAPI. Scale bars, 25 µm. Synapsin and MAP2 intensity values are normalized to CON condition (standard deviations and *P*-values indicated on graphs; one-way ANOVA with multiple comparisons and Fisher's LSD test; *n*=5-10 mice with one field of view/animal/condition). (**I-K**) Representative images (**I**) and quantification (**J, K**) of TOMA-1 (green) and MitoSOX (red) fluorescence intensity in hippocampal area CA1 from mice treated as indicated. Scale bars, 50 µm. Intensity values are normalized to DEX condition (standard deviations and *P*-values indicated on graphs; one-way ANOVA with multiple comparisons and Fisher's LSD test; *n*=6 mice/condition for **J, K**).

Figure 7 Mifepristone or mito-apocynin rescue mitochondrial dysfunction and Tau pathology in Alzheimer's cybrid cells. (**A-D**) Representative images (**A**) and quantifications (**B-D**) of oligomeric Tau (Tau22; green), MitoSOX (red), and AT8 (grey) fluorescence intensity for differentiated SH-SY5Y control (nonAD) and Alzheimer's disease subject (AD) cybrid cells treated with vehicle (CON), MIF, or mAPO. Scale bar, 25 µm. Intensity values are normalized to control for AT8 and MitoSOX, and to Alzheimer's control condition for Tau22 due to the absence of Tau22 immunostaining in non-Alzheimer's cybrid cells (standard deviations and *P*-values

indicated on graphs; one-way ANOVA with multiple comparisons and Fisher's LSD test, *n*=8 fields of view from 4 cybrid cell lines/condition). **(E)** Area of Tau22 colocalization with MitoSOX, normalized to AD control condition (standard deviations and p values indicated on graphs; one-way ANOVA with multiple comparisons and Fisher's LSD test; *n*=8 fields of view from 4 cybrid cell lines/condition). (**F-G**) Complex I activity (**F**) and ATP levels (**G**) in cybrid cells treated as indicated, normalized to CON condition (standard deviations and *P*-values indicated on graphs; one-way ANOVA with multiple comparisons and Fisher's LSD test; *n*=3-4 independent cybrid cell lines/condition).

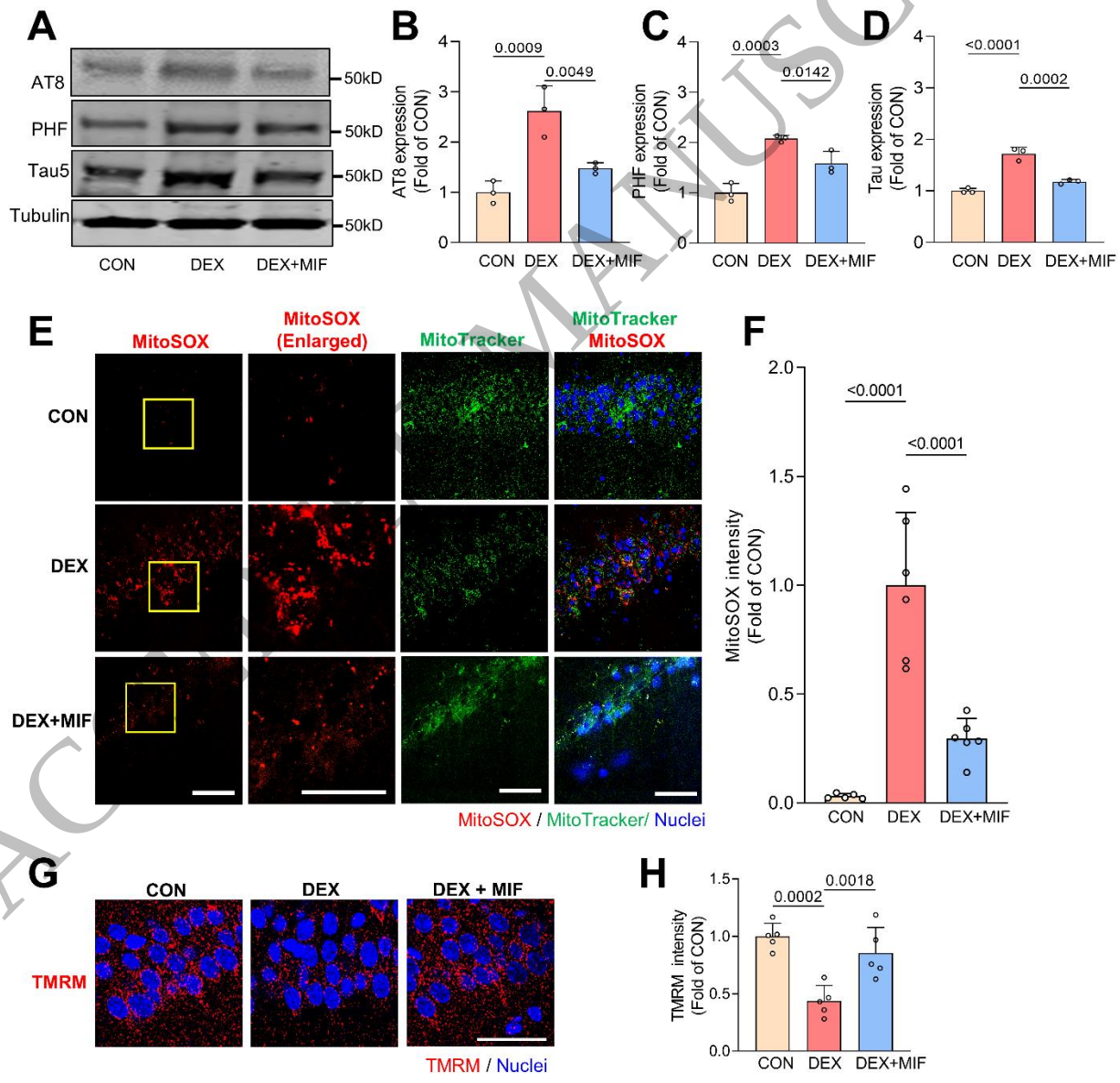

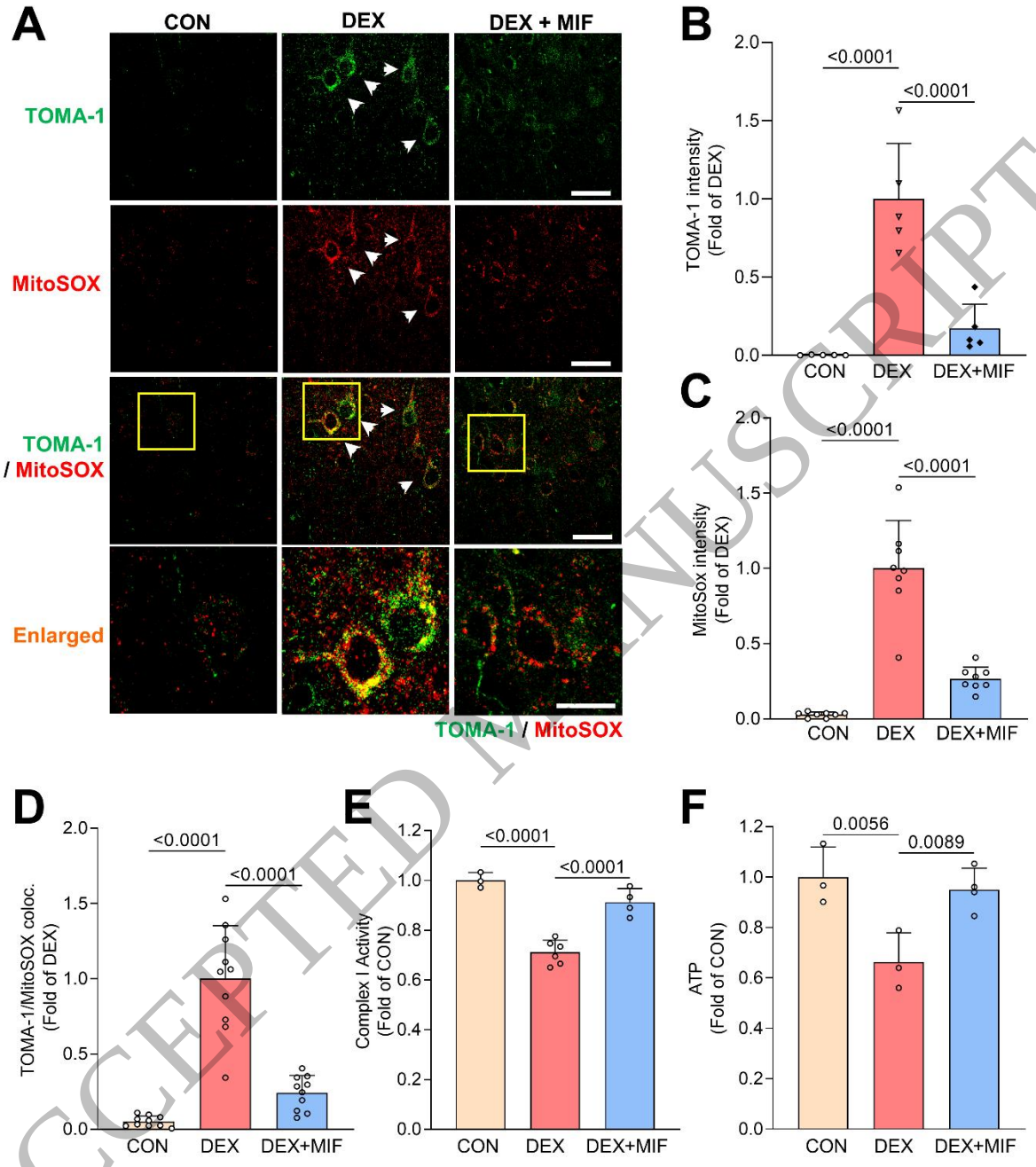

1

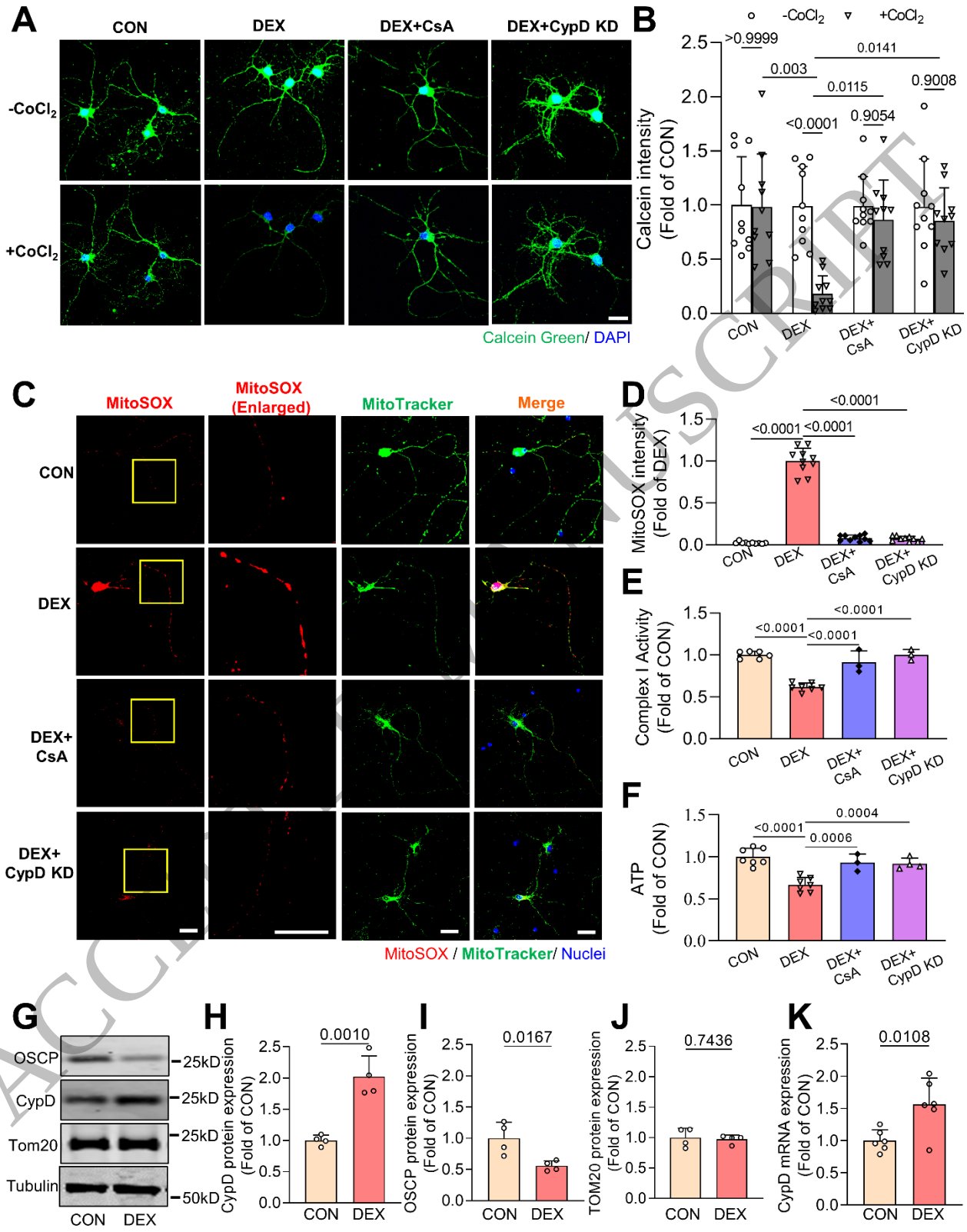

1

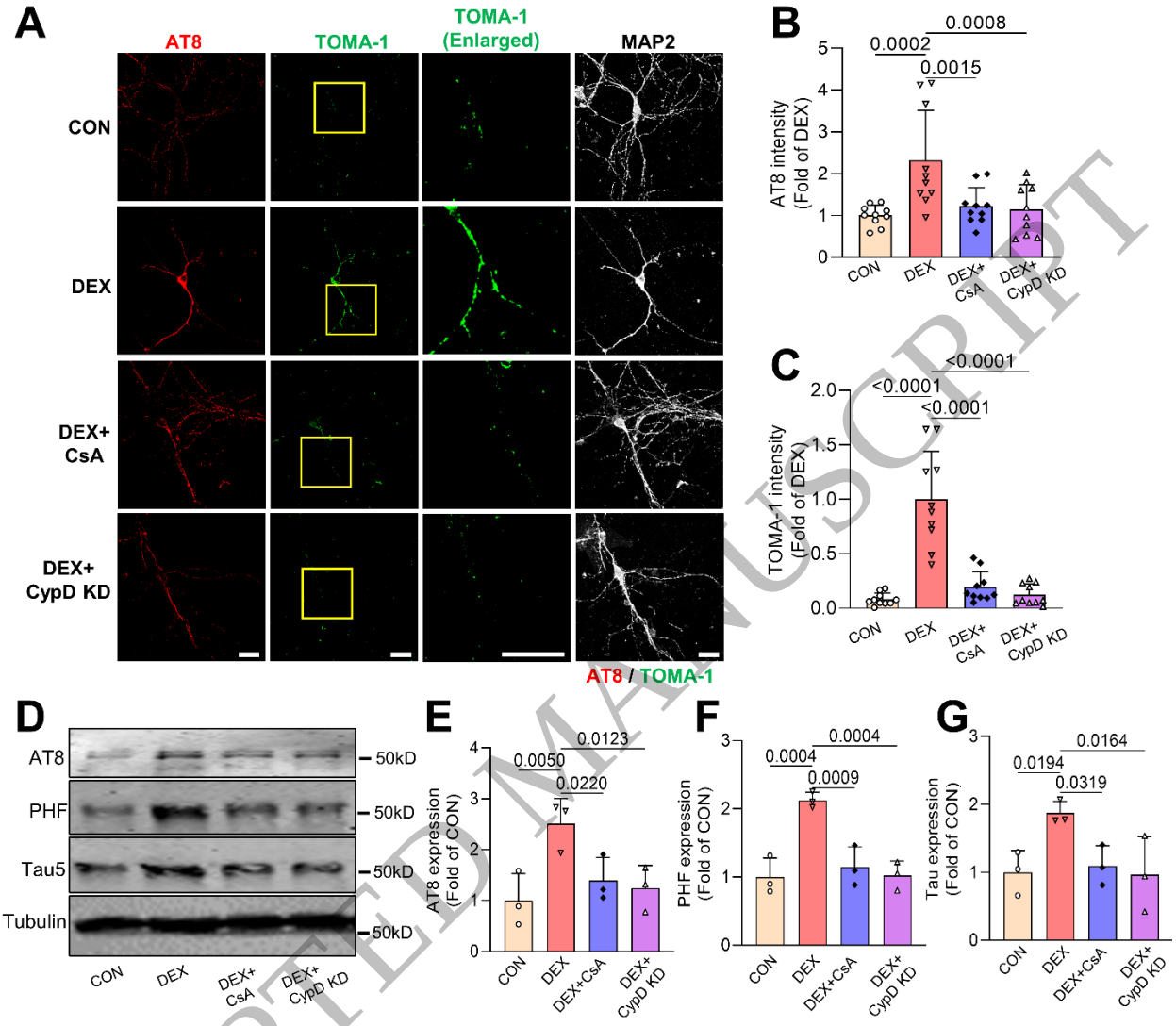

1

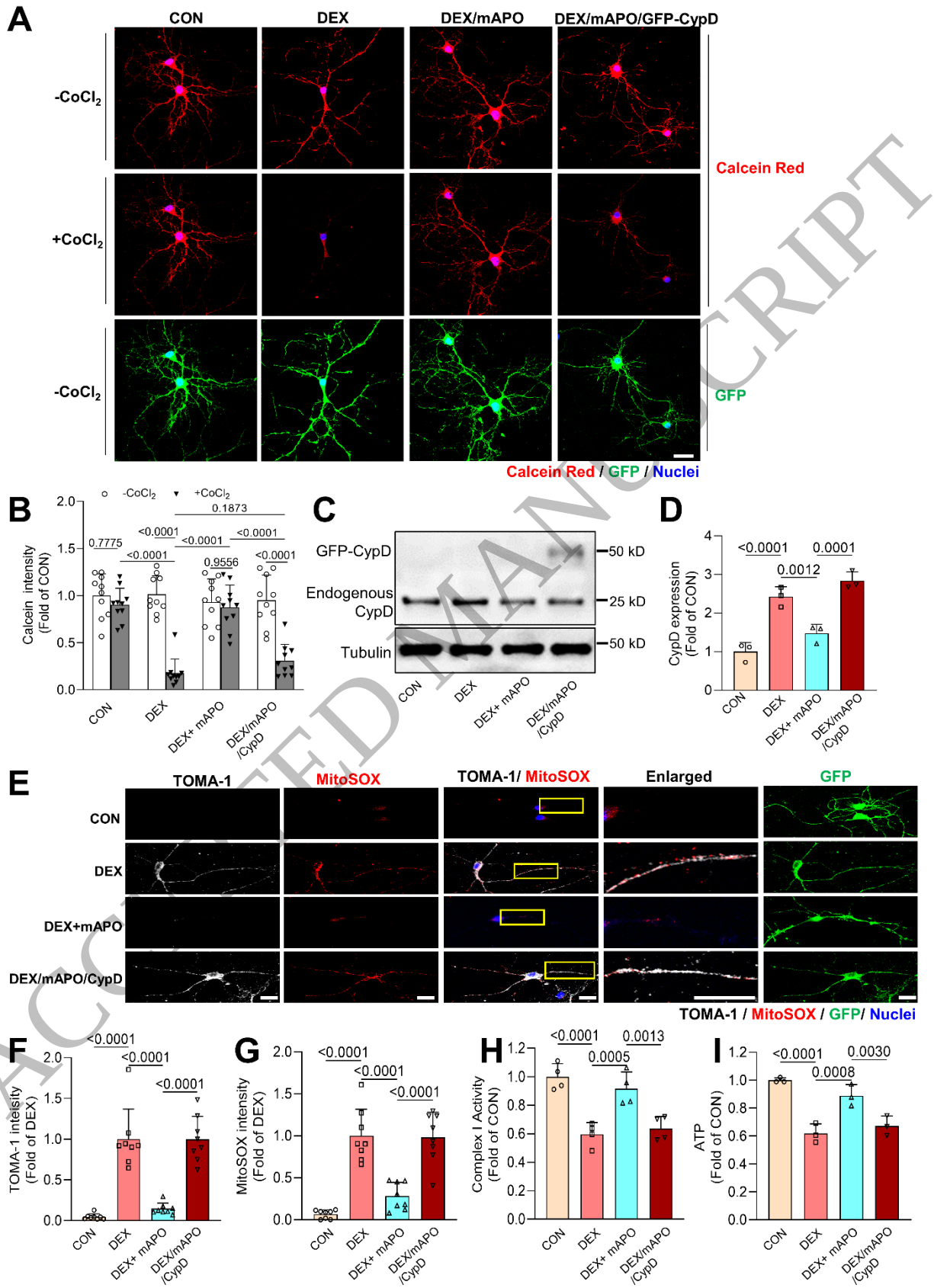

1

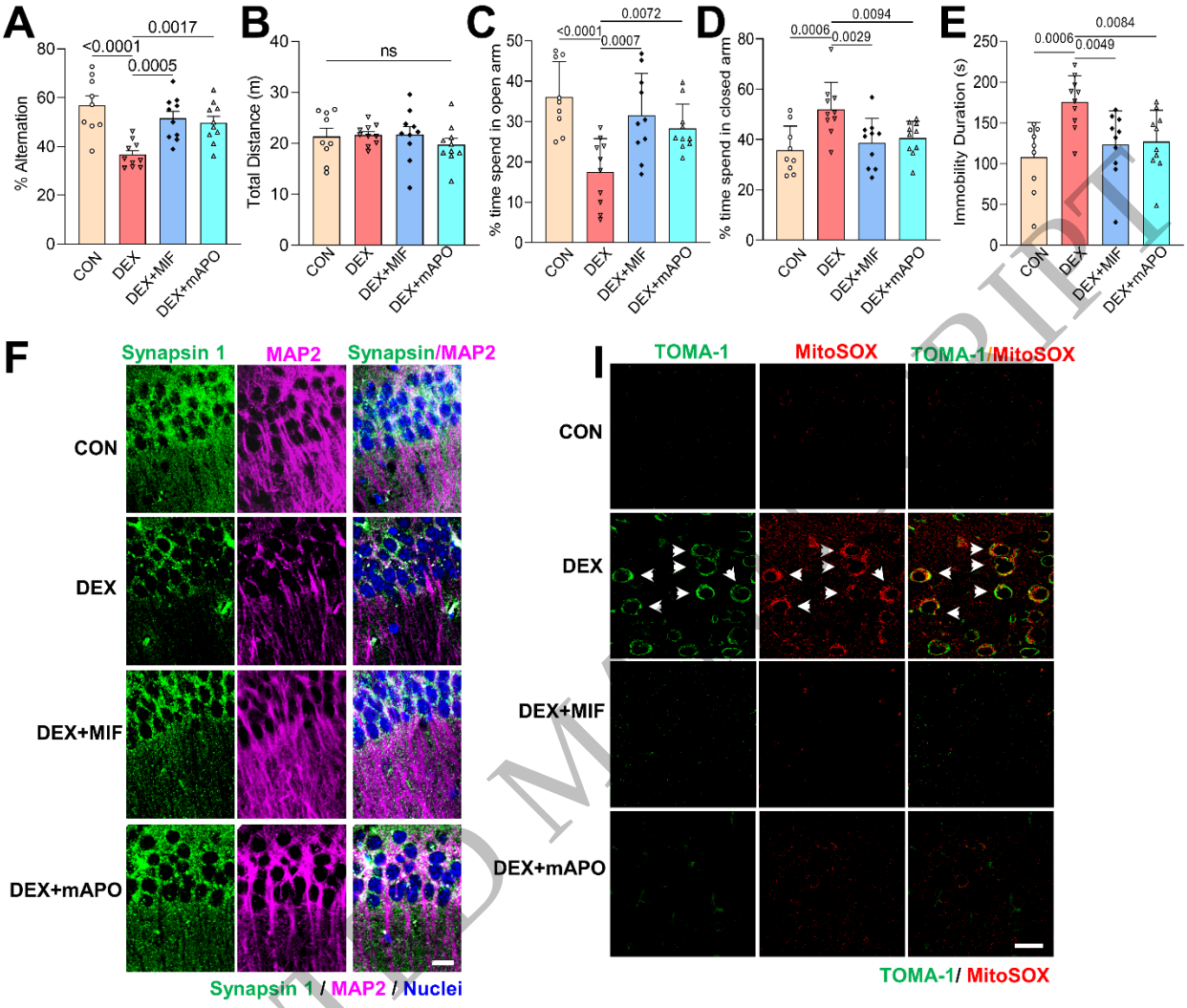

1

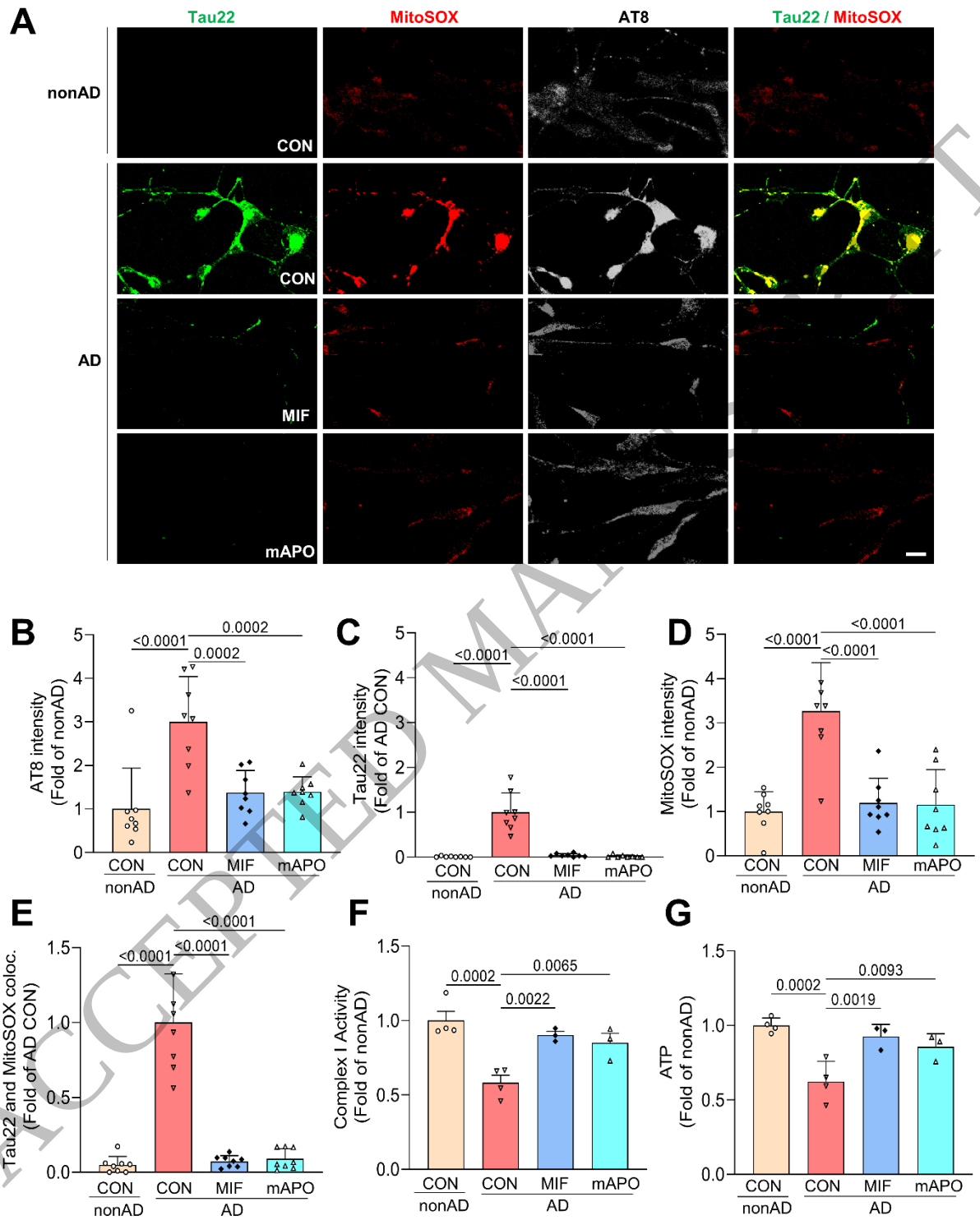

1